# A Novel Constant Volume System for Determining Transport Properties in Polymeric Membranes

**By**

**Peter Jr. Leszczynski**

**Supervisor**

**Boguslaw Kruczek, P.Eng., PhD**

**Thesis submitted to the University of Ottawa**
**in partial Fulfillment of the requirements for the**
**Master of Applied Science in Chemical Engineering**

**Department of Chemical & Biological Engineering**
**Faculty of Engineering**
**University of Ottawa**

**Abstract**

Membrane gas separation became an industrial reality in the late 1970s with Monsanto's first commercial asymmetric hollow fiber membrane modules. Innovations in membrane separations result from new materials that exhibit an improved permeability and are more selective than their predecessors, with materials commonly compared to the "upper bound line." Accurate determination of the three transport properties which characterize a membrane, permeability (*P*), diffusivity (*D*), and solubility (*S*), is thus of great interest to exceed the current upper bound line. Also, proper characterization of membrane materials enables enhancing current commercial membrane processes or allows for new applications.

All three transport properties, *P*, *S*, and *D,* can be determined using a single dynamic gas permeation experiment in a constant volume (CV) system, commonly called the time-lag method. This work presents the next-generation CV system that utilizes the two-tank volume concept, namely a reference volume and a working volume. Compared to the previous iteration, the pressure in the reference volume can be reduced to the anticipated pressure in the working volume after initiating the gas permeation experiment. This allows monitoring of the pressure decay in the working volume (i.e., gas permeation into the membranes) using a high-resolution differential pressure transducer (DPT) right after initiating the experiment. The new system's operation is demonstrated by simultaneous monitoring of the upstream pressure decay and the downstream pressure rise during the time-lag experiments using a polyphenylene oxide (PPO) membrane. The values determined using the pressure decay method are compared to those determined using the downstream method to identify any limitations still present in the current iteration of the CV system.

To set a reliable benchmark value to compare against, the downstream receiver was redesigned, and an optimal configuration was identified, which was associated with negligible resistance to gas accumulation and, thus, a minor error in the experimental time lag downstream from the membrane. Furthermore, a temperature enclosure was built to minimize errors caused by the constant temperature assumption during the time lag analysis. Additionally, the temperature-controlled enclosure allows for transport properties temperature dependence to be quantified by determining the activation energy of permeability, diffusion, and the enthalpy of solution for a given gas/polymer system.

**Résumé**

La séparation des gaz l'aide de membranes est devenue une réalité industrielle à la fin des années 1970 avec les premiers modules commerciaux composés de membranes tubulaires asymétriques développés par Monsanto membrane creuse asymétrique de Monsanto. Les innovations dans les séparations membranaires résultent de nouveaux matériaux qui présentent une perméabilité améliorée et sont plus sélectifs que leurs prédécesseurs, avec des matériaux couramment comparés à la "ligne limite supérieure". La détermination précise des trois propriétés de transport qui caractérisent une membrane, la perméabilité (P), la diffusivité (D) et la solubilité (S), est donc d'un grand intérêt pour dépasser la limite supérieure actuelle. En outre, une caractérisation appropriée des matériaux membranaires permet d'améliorer les procédés membranaires commerciaux actuels ou permet de nouvelles applications.

Les trois propriétés de transport, P, S et D, peuvent être déterminées à l'aide d'une seule expérience dynamique de perméation d'un gaz dans un système à volume constant (CV), communément appelée la méthode du décalage temporel. Ce travail présente le système CV de nouvelle génération qui utilise le concept de volume à deux reservoirs: Un volume de référence et un volume de travail. Par rapport à l'itération précédente, la pression dans le volume de référence peut être réduite à la pression anticipée dans le volume de travail après le lancement de l'expérience de perméation de gaz. Cela permet de surveiller la décroissance de la pression dans le volume de travail (c'est-à-dire la perméation de gaz dans les membranes) à l'aide d'un transducteur de pression différentielle haute résolution (DPT) juste après le début de l'expérience. Le fonctionnement du nouveau système est démontré par la surveillance simultanée de la décroissance et de l'augmentation de la pression pendant les expériences de décalage temporel à l'aide d'une membrane d'oxyde de polyphénylène (PPO). Les valeurs déterminées à l'aide de la méthode de décroissance de la pression sont comparées à celles déterminées à l'aide de la méthode en aval pour identifier les limitations encore présentes dans l'itération actuelle du système CV.

Pour définir une valeur de référence fiable à comparer, le récepteur en aval a été repensé et une configuration optimale a été identifiée, associée à une résistance négligeable à l'accumulation de gaz et, par conséquent, à une erreur mineure dans le décalage temporel expérimental en aval de la membrane. De plus, le système a été placé dans une enceinte isolée thermiquement pour minimiser causées par l'hypothèse de température constante lors de l'analyse du décalage temporel. De plus, l'enceinte à température contrôlée permet de quantifier la dépendance à la température des propriétés de transport en déterminant l'énergie d'activation de la perméabilité, de la diffusion et de l'enthalpie de solution pour un système gaz/polymère donnè.

**Statement of Contributions**

I hereby declare that this work has not been submitted or accepted for any other degree. Dr. Boguslaw Kruczek supervised the research performed in this thesis.

**Chapter 2**: The constant volume system displayed in Chapter 2, and used to gather all data used for this thesis was modified together with Haoyu Wu. Together we redesigned the configuration of the apparatus, and I further improved the design by adding temperature control.

**Chapter 3:** Siamak Lashkari developed the analytical model used to predict the expected time lag contribution of the downstream receiver. I corresponded with him to check over my simulator to ensure it was functioning correctly.

## Table of Contents

## List of Figures

## List of Tables

## 1.0 Introduction

Membrane gas separation became an industrial reality in the late 1970s with Monsanto's first commercial asymmetric hollow fiber membrane modules [1]. Today's prominent membrane-based gas separations include hydrogen recovery [2], natural gas purification [3] and air separation [4]. In addition, olefin/paraffin separations, ethanol/water separations, and carbon capture applications have expanded the opportunities for gas separation membranes [5]. Despite significant progress in the development of inorganic [6] and mixed matrix membranes (MMMs) [7], commercial gas separation membranes are typically made from synthetic organic polymers. These include polysulfones, cellulose acetates, polyphenylene oxide, aramids, polycarbonates, and polyimides [5]. Developing new materials - organic, inorganic, and composite – remains the central theme of membrane gas separation research. The combination of permeability and permselectivity for a given pair of gases compared to the upper-bound line is the standard metric for assessing new membrane materials [8]. In turn, permeability ($P$) and permselectivity for a given pair of gases depend on the respective diffusivity ($D$) and solubility ($S$) coefficients of these gases in the membrane material. The three transport coefficients, $P$, $D$, and $S$, can be determined in a single dynamic gas permeation experiment, often referred to as a time-lag experiment. The mathematical basis for the time lag experiment was first described more than a century ago [9].

### 1.1 Downstream time-lag method

Time-lag experiments are generally performed in constant volume (CV) systems. A degassed, homogeneous membrane from the tested material is exposed to a step pressure increase at one (feed) side. The resulting pressure rise at the other (permeate) side of the membrane is monitored in real-time. The tangent of the linear portion of the pressure rise is directly proportional to the downstream permeability ($P_d$) [10]. The extrapolation of that linear portion to the time axis yields a downstream time lag ($\theta_d$) [10], which is related to the diffusivity by Eq. (1):

$$\theta_d = \frac{L^2}{6D} \tag{1}$$

where $L$ is the membrane thickness. According to the solution-diffusion model, the ratio of $P$ and $D$ represents $S$ [11] described by Eq (2):

$$S = \frac{P}{D} \tag{2}$$

Eq. (1) is valid when gas sorption follows Henry's law and for the ideal boundary conditions [10]. The latter includes the assumption that gas concentration at the permeate interface of the membrane is zero during the entire experiment [12]. As the gas accumulates at a downstream receiver of the CV system, the gas concentration at the permeate interface of the membrane increases. It is possible to consider the effects of gas accumulation [11,12–14]. However, the resulting equivalent of Eq. (1) loses its simplicity and is practically not used by the researchers. Moreover, the errors arising from applying Eq. (1) in properly designed CV systems should be insignificant [15,16]. $P$ can be calculated using the experimentally determined pressure response in the downstream receiver $dp_d/dt$ using Eq. (3) [17]:

$$P = \frac{V_d L}{p_0 A_m R T} \frac{dp_d}{dt} \tag{3}$$

where $V_d$ is the volume of the downstream receiver, $L$ is the thickness of the membrane sample, $p_0$ is the feed pressure, $A_m$ is the area of the membrane, $R$ is the universal gas constant, and $T$ is the absolute temperature.

### 1.2 Time lag contribution of the downstream receiver

The accumulation of gas emerging from the membrane in a high-vacuum constant volume system may be associated with a resistance that influences the observed time lag [18-20]. The distribution of accumulated gas within the permeate collector can be described as a diffusive process with a constant diffusivity [18-20]. Permeate collectors within CV systems typically consist of small diameter tubing (1/8-1/2") tubing and/or additional volumes [20]. Since the downstream receiver is initially at a high-vacuum, and tube diameters tend to be small, collisions between gas molecules and tube walls are more probable than intermolecular collisions. The result of the frequent wall collisions relative to intermolecular collisions results in a Knudsen flow regime. It is commonly accepted that Knudsen diffusion occurs when $r/\lambda < 0.1$ where $r$ is the tube/pore radius, and $\lambda$ is the mean free path of gas molecules described by Eq. (4) [18].

$$\lambda = \frac{1}{\sqrt{2}\pi d^2 n} \tag{4}$$

where $d$ is the molecular diameter, $n$ is the molecular concentration described by Eq. (5).

$$n = \frac{pN_A}{RT} \tag{5}$$

where $N_A$ is Avogadro's constant. The Knudsen diffusion coefficient ($D_k$) can be calculated using Eq. (6) [18].

$$D_k = \frac{2}{3} r \sqrt{\frac{8RT}{\pi M}} \tag{6}$$

where $M$ is the molecular mass of the gas.

Assuming a constant diffusion coefficient, the governing equation describing the flow of gas within the downstream receiver is Fick's second law of diffusion [18]. For the simplest case, where the permeate receiver is a single tube, the position dependent time lag contribution of the receiver ($\theta_Z$) can be described by Eq. (7) [18].

$$\theta_z = \frac{Z_n^2}{6D_k} - \frac{(Z_n - x)^2}{2D_k} \tag{7}$$

where $Z_n$ is the total length of the permeate tube, and $x$ is the distance from the membrane.

At $x = 0$, and $x = Z_n$, the time lag of the single tube receiver corresponds to the inlet and outlet time lags of a membrane [18]. The analogous time lag expressions result from the fact both gas diffusing through the membrane, and gas diffusing through the receiver were described as a one-dimensional media characterized by a constant diffusivity [18]. Maximal negative time lag contributions occur at $x = 0$, the membrane face, and the largest positive error occurs at the end of the permeate collector $x = Z_n$.

$$\theta_z(x = 0) = -\frac{Z_n^2}{3D_k} \tag{8}$$

$$\theta_z = \frac{Z_n^2}{6D_k} \tag{9}$$

This analysis of receiver time lag contribution was first extended from the case of a single tube to a tube with a single accumulation tank [19], and then further extended to a general model with any number of tanks [20]. The extended general analytical model developed for a receiver that consists of a main tube with $n$-1 junctions is described by Eq. (10) – Eq. (15).

The dimensionless time lag within the main tube of the receiver at junction $i$ ($\theta_i/\theta_0$) is equal to:

$$\frac{\theta_i}{\theta_0} = \frac{\Upsilon}{\theta_0} + \frac{\Psi}{\theta_0} - 3\left(\frac{Z_n - x}{Z_n}\right)^2 - 6\sum_{j=i}^{n-1}\left(\frac{A_{v_j} H_j + V_j}{AZ_n}\right)\left(\frac{Z_j - x}{Z_n}\right) \tag{10}$$

where, $\Upsilon$ is a position independent time lag contribution of the receiver Eq. (15), $\psi$ is a position

independent time lag contribution of the receiver Eq. (14), $A$ is the cross sectional area of the main tube, $A_{v_j}$ is the cross sectional area of the branches connecting to the main tube at junction $j$, $H_j$ is the overall height of the branch at junction $j$, $V_j$ is volume of the additional tank located at junction $j$, and $Z_j$ is the distance from the membrane to the junction $j$.

The dimensionless time lag within branch at junction $i$ ($\theta_{v_i}/\theta_0$) is equal to:

$$\frac{\theta_{v_i}}{\theta_0} = \frac{\theta_i\left(x = Z_i\right)}{\theta_0} + 3\frac{D_k}{D_{k,vi}}\frac{H_i\left(H_i + 2\left(V_i/A_{vi}\right)\right)}{Z_n^2} - 3\frac{D_k}{D_{k,vi}}\left(\left(\frac{H_i - y_i}{Z_n}\right)^2 + 2\frac{V_i}{A_{vi}Z_n}\frac{\left(H_i - y_i\right)}{Z_n}\right) \quad (11)$$

where $D_{k,vi}$ is the Knudsen diffusion coefficient of the gas in branch $v_i$, and $y_i$ is the height within branch $i$ at which the dimensionless time lag is being evaluated at, and $\theta_0$ is described by Eq. (12). where,

$$\theta_0 = \frac{Z_n^2}{6D_k} \quad (12)$$

$$\frac{\theta_i\left(x = Z_i\right)}{\theta_0} = \frac{\Upsilon}{\theta_0} + \frac{\Psi}{\theta_0} - 3\left(\frac{Z_n - Z_i}{Z_n}\right)^2 - 6\sum_{j=i}^{n-1}\left(\frac{A_{v_j}H_j + V_j}{AZ_n}\right)\left(\frac{Z_j - Z_i}{Z_n}\right) \quad (13)$$

$$\frac{\Psi}{\theta_0} = 6\frac{V_T}{AZ_n}\sum_{j=1}^{n-1}\left(\frac{A_{v_j}H_j + V_j}{V_T}\right)\sum_{k=j+1}^{n-1}\left(\frac{A_{v_k}H_k + V_k}{V_T}\right)\left(\frac{Z_k - Z_j}{Z_n}\right) \quad (14)$$

$$\frac{\Upsilon}{\theta_0} = \frac{AZ_n}{V_T} - 6\sum_{j=1}^{n-1}\frac{DA_{v_j}H_j}{D_{v_j}V_T}\left(\frac{1}{3}\left(\frac{H_j}{Z_n}\right)^2 + \frac{V_jH_j}{A_{v_j}Z_n^2} + \left(\frac{V_j}{A_{v_j}Z_n}\right)^2\right) + 3\sum_{j=1}^{n-1}\left(\frac{A_{v_j}H_j}{V_T} + \frac{V_j}{V_T}\right)\left(\frac{Z_j^2 + \left(Z_n - Z_j\right)^2}{Z_n^2}\right) \quad (15)$$

where $V_T$ is the total volume of the receiver. For a system with a single tank $\Psi/\theta_0 = 0$.

### 1.3 Upstream time-lag method

Following a step-change in feed pressure, the time-lag method could also rely on monitoring pressure decay in a constant volume upstream from the membrane. The corresponding expression for the upstream time lag ($\theta_u$) is given by [12]:

$$\theta_u = -\frac{L^2}{3D} \quad (16)$$

However, the standard way to determine the time lag in CV systems remains to monitor the pressure rise and thus utilize Eq. (1) [21]. The usefulness of using pressure decay measurements for the characterization of membrane materials was discussed by Nguyen et al. [22]. They compared $P$ and $D$ of dense and asymmetric PVTMS membranes determined using different characterization techniques, including the conventional time-lag and the decay rate measurement methods; the two methods yielded comparable values [22]. However, using pressure decay measurement can offer some unique advantages, particularly when characterizing barrier materials for which reaching the steady state permeation (necessary to determine the time lag) could take not seconds or minutes but hours or even days. Combining upstream pressure decay with downstream pressure rise allowed Al-Ismaily et al. to determine $P$ from transient permeation data before reaching a steady-state [23]. Immediately after initiating the gas permeation experiment, the membrane behaves as a semi-infinite solid. It can be shown that during that time, the pressure decay ($\Delta p_u$) is a linear function of the square root of time [23]:

$$\Delta p_u = -\frac{2 p_u SRTA\sqrt{D}}{V_u \sqrt{\pi}} \sqrt{t} \tag{17}$$

where $p_u$ is the upstream (feed) pressure, $V_u$ is the constant upstream volume, $A$ is the membrane area, $T$ is the absolute temperature, and $R$ is the universal gas constant. Eq. (17) implies that $\Delta p_u << p_u$. The slope of $\Delta p_u$ vs $\sqrt{t}$ is directly proportional to $S\sqrt{D}$, but the intercept from Eq. (17) is zero. Therefore, $S$ and $D$ cannot be determined from the initial pressure decay. However, it was shown that laminating the tested membrane with a film of known properties (e.g., silicone rubber) results in an intercept that depends on the tested membrane's $S$ and $D$ [24]. Therefore, the mathematical expression for the intercept yields the second independent equation, thus allowing determination $D$, $S$ and $P$ from the upstream pressure decay before the gas leaves the tested barrier material. It can also be shown that if the tested membrane is not laminated and the gas emerges from the membrane, the deviation from the initial linear relation given by Eq. (17) at any time depends on $D$ but not $S$ [25]. Therefore, $D$ can be evaluated from the observed deviation at the specific time, and knowing $D$, $S$ can be determined from the initial slope of $\Delta p_u$ vs $\sqrt{t}$.

Despite the potential advantages of monitoring pressure decay in membrane characterization, this approach did not gain much attention in the membrane community. There are two main reasons for that. The measurements in CV system rely on accurate monitoring of

pressure in time ($dp/dt$) using an absolute pressure transducer. Typically, the resolution of a high-quality absolute pressure transducer is 1/10,000 of its maximum reading. When monitoring pressure rise starting from a high vacuum, it is sufficient to use the pressure transducer with a maximum reading of 1 Torr with the corresponding resolution of 0.0001 Torr. On the other hand, a pressure transducer with a maximum reading of 1000 Torr would be required to monitor pressure decay in a time-lag experiment. The corresponding resolution of 0.1 Torr might be insufficient when characterizing low-permeability materials. It is also assumed that measured $dp/dt$ in a CV system arises only from the gas's molar flow ($dn/dt$) into or out of the membrane. It is a reasonable assumption when monitoring pressure rise starting at high vacuum ($p \approx 0$), but not necessarily when monitoring the pressure decay after initiating a time-lag experiment, which is evident when considering the total derivative from the ideal gas law:

$$\frac{dp}{dt} = \frac{RT}{V}\frac{dn}{dt} - \frac{p}{V}\frac{dV}{dt} + \frac{p}{T}\frac{dT}{dt} \tag{18}$$

The second term on the right-hand side is always assumed to be zero. However, when monitoring the pressure decay, the last term on the right-hand side might not be non-zero even when the temperature is controlled because of the magnitude of feed pressure ($p >> 0$). It is important to note that monitoring pressure decay, referred to as a barometric method, is commonly used to determine the $S$ and $D$ of adsorbents, including polymer membranes [26].

Al-Ismaily et al. [23] addressed the resolution problem of absolute pressure transducers by adopting the concept of a two-tank volume developed by Arkilic et al. [27]. This concept is commonly used in microfluidics. In a two-tank volume system, one tank is a reference volume, and the other is a working volume. The microflow into the working volume is measured by comparing the resulting pressure increase to the constant reference volume pressure using a differential pressure transducer (DPT). Similarly, to absolute pressure transducers (APT), the resolution of DPT is related to the maximum reading, which can be very small, increasing the resolution of the measured $dp/dt$. Because time-lag experiments are initiated by sudden pressurization of a membrane, the working volume must be further split into two volumes to isolate the membrane (keep it at a high vacuum). The latter includes the upstream part of the membrane cell and tubing, which can be referred as a dead volume. Regardless of how small the dead volume is, starting the gas permeation experiment results in an expansion in the working volume, which is much greater the maximum reading of DPT. Therefore, Al-Ismaily et al. [23] initiated gas

permeation experiments when the reference and working volumes were connected. The two volumes were separated, and pressure decay started to be monitored only after a few seconds from the pressurization of the tested membrane.

### 1.4 Thesis objectives

Three are mainly three objectives for the research in this thesis. The objectives include:

1. Improve the design of the constant volume system in our lab and identify the configuration of the downstream receiver which provides the most accurate measure of transport properties. The accurate determination of transport properties using the downstream receiver is critical for setting benchmark values to allow comparison using the novel technique of characterizing polymeric using a single dynamic gas permeation experiment based on the rate of pressure decay in the high-pressure working volume.
2. Add the capability of performing time-lag experiments at various temperatures to allow for determination of the activation energy of permeation, diffusion, and heat of solution for a gas/polymer system.
3. Characterize a polymeric material using upstream pressure decay and compare the transport properties determined using the upstream method to those determined using pressure rise within the accurate downstream configuration to identify any limitations currently exhibited by the novel constant volume system.

### 1.5 Outline of the thesis

The structure of the thesis is formatted as such:

1. The first chapter is the introduction which outlines the theoretical background required to achieve the three objectives outlined.
2. The second chapter is an overview of the current iteration of the constant volume system and provide the experimental protocols used to achieve the objectives outlined.
3. The third chapter studies the time lag contribution of the downstream permeate collector and identify the configuration which imparts the lowest time lag contribution.
4. The fourth chapter uses the newly added temperature control capabilities to conduct gas permeation experiments at various temperatures to measure the activation energy of permeation, diffusion, and the enthalpy of solution.

5. The fifth chapter examines two methodologies by which the raw data collected during the upstream pressure decay experiment can be adjusted to recover meaningful data and use this data to characterize a polyphenylene oxide membrane. A comparison is made between the results gathered using the well-established downstream time lag experiments with the results of the novel method for characterizing membranes.
6. The sixth chapter is a general conclusion and recommendations to improve the performance of the upstream pressure decay functionality of the constant volume system presented.

## 2.0 Constant Volume System Overview and Experimental Protocols

The current evolution of the CV system used to characterize membranes leveraging the time-lag method is illustrated in Figure 1. The CV system presented in this chapter is an evolution of the previous iterations [17][23] which had the novel feature of being able to perform the time lag experiment using upstream pressure decay. The current iteration has been designed to address limitations of prior versions [17]. This chapter presents a general overview of the system capabilities and provides design heuristics and design choices made when developing this iteration.


*Figure 1 - Picture of the constant volume system.*

A scale schematic of the CV system pictured in Figure 1 is represented by Figure 2.

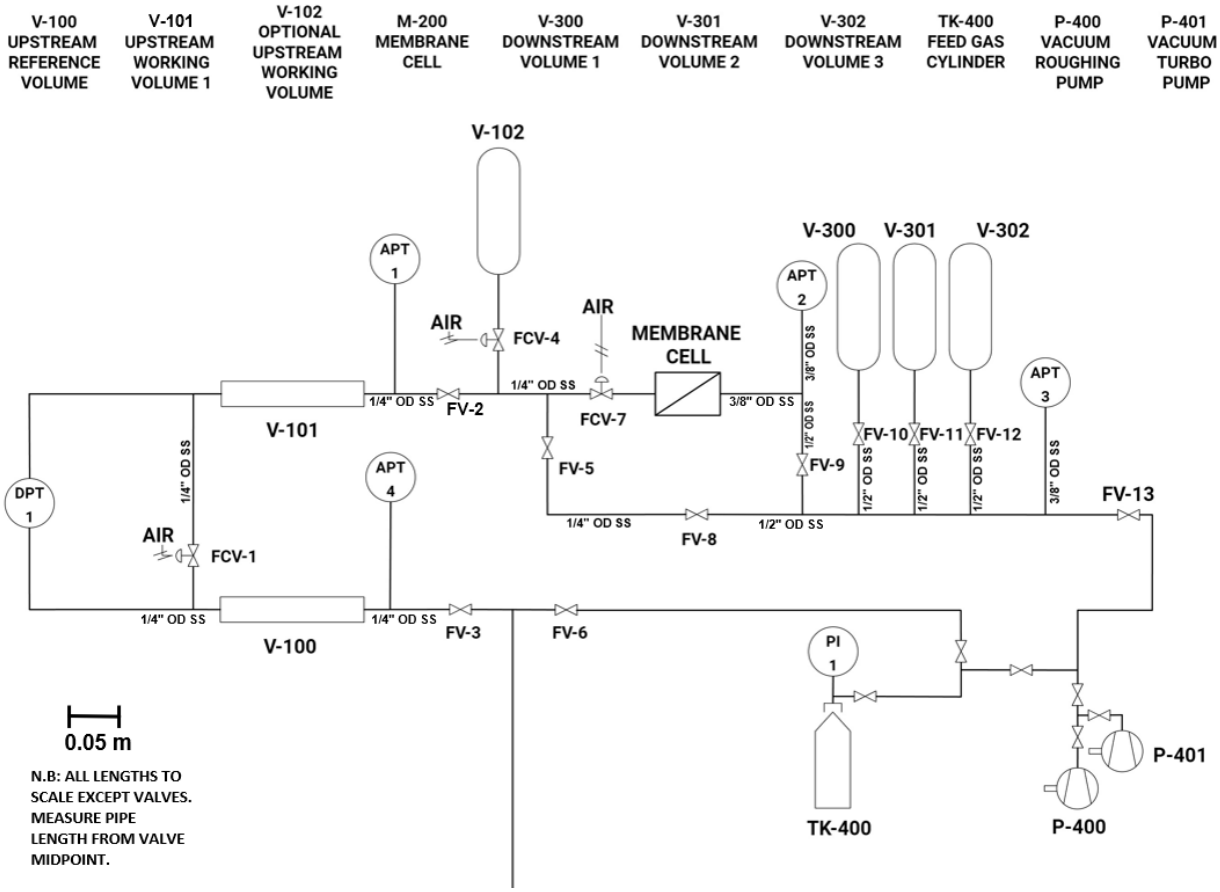


*Figure 2 - Schematic of the Constant Volume system.*

The CV system presented in Figure 2 is comprised of three distinct sections; the upstream section bounded by valves FV-3, FV-5 and FCV-7, the membrane cell, and the downstream receiver bounded by the membrane cell, FV-8, and FV-13. The downstream features three additional volumes (V-300, V-301, and V-302) that can easily be included or excluded from the downstream section using FV-10 through FV-12. Membranes are characterized by monitoring the pressure rise response to a step-change in pressure with $APT_2$ and $APT_3$. The upstream portion of the CV system has 3 components which provide the core of its functionality, to be able to supply feed gas to the membrane and monitor the pressure decay rate within the working volume. The pressure decay is measured by means of a pressure differential between V-100 and V-101 measured with a capacitance based differential pressure transducer (DPT) (CCR Process Products Kanata, Ontario, Canada, MKS698A ±1 Torr, $10^{-6}$ full scale resolution, accuracy: 0.05% of reading).

### 2.1 Downstream capabilities

1. Adjustable downstream receiver configuration and volume allows for appropriate volumes selection when characterizing membranes. Too large of a receiver volume will reduce the sensitivity of the CV system. This is especially true for materials with low permeability or thick films. FV-9 can be closed, and pressure rise can be observed with the 10 Torr absolute pressure transducer (CCR Process Products Kanata, Ontario, Canada, MKS627F11TBC1B, $10^{-5}$ full scale resolution, accuracy: 0.12% of reading, range: 0 to 10 Torr). Valve FV-9 is located 0.165 m downstream of the membrane and limits the downstream receiver volume ($V_T$) to $2.84 \times 10^{-6}$ $m^3$. Alternatively, for highly permeable gases the downstream volume can be expanded by the inclusion of accumulation tanks V-300-V302 that are attached to the main line of the receiver.
2. The time lag contribution of the downstream receiver can be studied through monitoring the pressure response with two independent absolute pressure transducers, $APT_2$ and $APT_3$ located 0.095 and 0.519 m from the membrane respectively. Receiver configurations can easily be altered through actuation of valves FV-10, FV-11, and FV-12.

### 2.2 Upstream capabilities

1. The upstream working and reference volumes can be isolated from each other with the valve FCV-1(Weston Valve & Fitting LTD, Mississauga, ON, Swagelok SS-4BK-VCR-1D & SS-4BK-1C-K10). This allows for a differential pressure transducer (DPT) to directly measure the pressure decay within the working volume and is the basis of the upstream time lag experiment conducted using the CV system presented. The DPT provides a much greater resolution than the $APT_1$ and $APT_4$ as its full-scale range is ±1 Torr which resolves $10^{-6}$ of full scale.
2. Absolute pressure can be measured in both the reference and working volumes independently using 2000 Torr pressure transducers $APT_4$ and $APT_1$ (CCR Process Products Kanata, Ontario, Canada, MKS627F13TBC1B, $10^{-5}$ full scale resolution, accuracy: 0.12% of reading, range: 0 to 2000 Torr).

3. Pressure can be reduced within the reference volume with the aid of P-400 and valves FV-3 and FV-6 to compensate for the pressure drop that occurs initially after initiating the time lag experiment by opening FCV-7.
4. Additional volume can be added to the working volume to keep a more constant feed pressure for characterizing highly permeable materials.

### 2.3 General system capabilities

**1.** A membrane bypass loop exists to allow for evacuation of membrane sample and dead volume.
**2.** Pneumatically actuated valves can be programed to open in any sequence and are controlled remotely. This allows for repeatable experiments using either methodology where FCV-1 is first closed isolating the two volumes prior to opening FCV-7, or the reverse where FCV-7 is opened first followed by isolation of the two volumes. Additionally, disturbances in the temperature withing the chamber housing the CV system are minimized by keeping the chamber sealed prior to initiating the time-lag experiment.
**3.** Most valve connections have been brazed to reduce possible sources of leaks. The remainder of the connections are sealed tight with metal gasket face seals.
**4.** The entirety (high- and low-pressure sides) can be exposed to vacuum using a roughing pump P-400 (CANVACTECH, Ottawa, Ontario, Canada, Edwards RV3, A65201906, ultimate pressure: $1.5 \times 10^{-3}$ Torr) and a turbomolecular pump P-401 (Edwards Vacuum LLC Sanborn, New York, USA, Edwards TS85D1002, ultimate pressure: $< 3.75 \times 10^{-10}$ Torr) to degas tube walls when switching feed gas or after installing a new membrane sample.
**5.** Temperature can be adjusted above and below ambient temperatures, allowing for activation energies of permeation, diffusion, and the heat of solution to be determined by performing time lag experiment at various temperatures.

### 2.4 Leak rates

The leak rates within the system can be quantified at either vacuum or above atmospheric pressures. Featuring 4 absolute pressure transducers, the system can be compartmentalized using the valves to quantify leak rates in specific parts of the system to identify where a leak

is occurring. Typical leak rates experienced within this CV system are presented in Table 1.

*Table 1 – Typical leak rates within the CV system.*

| Section | Bounds | Volume [m3] | Leak Rate [Torr/s] |
|---|---|---|---|
| Reference volume | FCV-1, FV-3 | $9.66 \times 10^{-5}$ | $6.0 \times 10^{-7}$ |
| Working volume | FCV-1, FV-4, FV-5, Membrane | $1.10 \times 10^{-4}$ | $9.0 \times 10^{-7}$ |
| Downstream volume, tubing only | Membrane, FV-8, FV-10, FV-11, FV-12, FV-13 | $8.13 \times 10^{-5}$ | $8.1 \times 10^{-8}$ |

The leak rates within each section are considered negligible as they are 4 and 5 orders of magnitude lower than the measured pressure decay and rise typically encountered within the upstream and downstream sections of the CV system during a membrane characterization trial.

### 2.5 Design considerations

Downstream of the membrane cell 12.7 mm (½") OD stainless steel tubing has been utilized to minimize the downstream receiver time lag contribution [18]. Larger tube diameters would further reduce the resistance to gas accumulation within the receiver, but 12.7 mm (½") was used as it was compatible with components already available in the lab. The absolute pressure transducers $APT_3$ have been placed at the end of the main tube in the downstream receiver as this position experiences a lesser time lag contribution from the receiver when additional volumes (V-300, V-301, V-302) are utilized. The location of $APT_2$ allows for monitoring pressure rise while FCV-9 is closed, minimizing the downstream volume. The range of the DPT has been increased from 0.2 Torr to ± 1 Torr to allow for upstream time lag experiments to be monitored for extended periods of time. Additionally, the extended range of the new DPT allows for permeation experiments to be performed at higher pressures using both methodologies where the two upstream volumes are isolated after, or prior to opening FCV-7. Previously, closing FCV-1 after FCV-7 would cause a compression effect resulting from a decrease in volume caused by the valve stem lowering, which would consume the range of the DPT at elevated pressures [17]. A brass insert is used within the downstream half of the membrane cell to minimize the dead volume.

### 2.6 Temperature control

A temperature-controlled enclosure was constructed to house the CV system to have a tighter control over the temperature. Previously the CV system was on a lab bench and was subject to a high degree of variability in ambient temperature. The temperature-controlled chamber can be

heated above or cooled below ambient temperatures. The range of temperatures achievable between both functionalities is 273-313 K. The system could be heated to a greater temperature but the APTs and DPT are heated internally and lose accuracy at temperatures greater than 313 K.

### 2.6.1 Heating

The heating of the enclosure which houses the CV system is achieved through a resistive heater located within ductwork. Air is continuously circulated using an inline fan and is recirculated by entering the air return vent and exiting through the register. The inline fan also draws a minimal amount of ambient air from the lab to constantly provide a process heat duty for the heater to oppose. Air temperature is monitored using two resistance temperature detectors (RTD) (Omega Sensing Solutions ULC, Arthur-Sauvé, Quebec, Canada, P-L-A-1/8-6-0-T-10, Class A: ±0.06% of resistance or ± 0.15°C at 0°C) one located between the two upstream volumes, and one measuring the heated air leaving the register. Using two RTDs cascade control is used where the set point of the temperature of the heated air leaving the register is adjusted to achieve a more stable temperature within the bulk of the air measured by the RTD located between both volumes. Using cascade control the temperature could be controlled to ±0.05 K, a 2 order of magnitude improvement of the ambient lab temperatures.

A picture depicting the heating system described is exhibited in Figure 3. Note that the cover for the heater enclosure was removed for this picture.

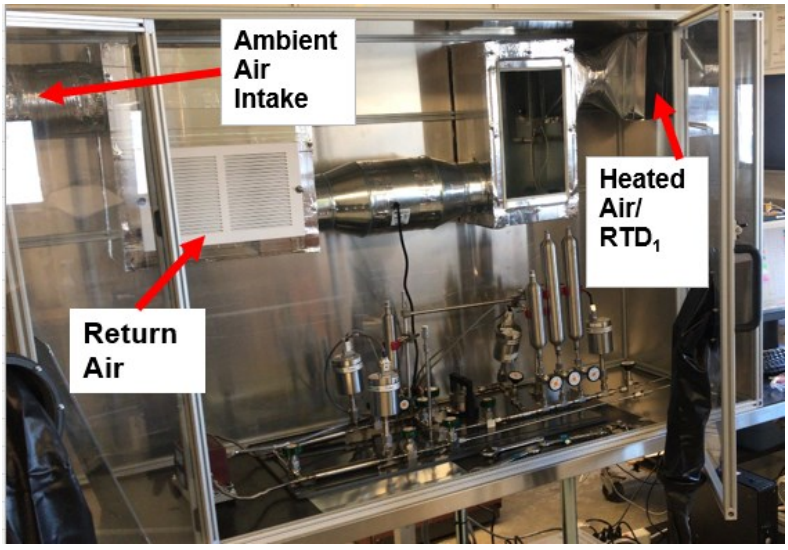


*Figure 3 - CV system within its temperature-controlled enclosure.*

### 2.6.2 Cooling

Cooling functionalities were added to the enclosure so that a wider range of temperatures could be used when performing time lag experiments. This gives the current CV system the capability to accurately determine activation energies of permeation, diffusion, and enthalpy of solution for gas/polymer systems. Cooling was achieved by installing an ordinary window air conditioning unit through the wall of the enclosure. Air conditioning units are typically limited to a minimum temperature of around 288 K, thus by adding a Coolbot controller (Store It Cold LLC Medley, Florida, USA, Coolbot Pro) the air conditioner could achieve temperatures as low as 273 K. The Coolbot controller measures the temperature of the air within the enclosure and uses a resistive heater to heat the thermistor of the air conditioner. This results in the air conditioner reading a greater temperature than is present within the chamber allowing for lower temperature setpoints to be achieved. Figure 4 shows the enclosure with the air conditioner, and Figure 5 shows the system after adding insulation. The system was insulated with R-15 rated insulation, and then covered with a reflective bubble wrap type insulation to reduce radiative heat transfer. Insulation was added for two reasons, to prevent condensation on the walls of the enclosure, and to keep temperatures below ambient condition more stable. The AC features a safety relay that sets a minimum amount of time that must pass before the compressor can be engaged after shutting off, this resulted in continuous cycling of temperature as the air conditioner is oversized for such a small enclosure. This limited the control of temperature significantly and resulted in oscillations in temperature of ±0.6 K when the cooling function was used.


*Figure 4 - Enclosure featuring the newly added air conditioning.*

*Figure 5 - Insulated enclosure with heating and cooling capabilities.*

### 2.7 Simultaneous upstream and downstream time-lag method experimental protocol

The experimental procedure outlined was utilized to perform the time lag experiment, monitoring the pressure decay and pressure rise response simultaneously. With the methodology presented, the reference and working volumes are isolated using FCV-1 prior to initiating the experiment by actuating FCV-7 just prior to the membrane cell.

1. The membrane sample is set to degas from the previous trial by closing FV-2, FV-4, and opening FV-5, FCV-7, FV-8, FV-9 and FV-13. If volumes V-300-V-302 are to be included in the downstream, then they must also be evacuated at the same time. This will increase the evacuation time required significantly.
2. With FV-2 closed, gas was fed from TK-400 at a pressure greater than the pressure desired for the time lag experiment into V-101, the working volume ($V_w$), and V-100, the reference volume ($V_r$). FV-3 was closed, and the gas was allowed to achieve thermal equilibrium with the air bath. The temperature of the gas was not directly measured; thus, it was left to equilibrate for a day as the membrane was degassing.
3. The membrane sample was evacuated until degassing could no longer be detected; this would typically take one day for a PPO membrane with a thickness of 47.5 μm if it had previously been installed in the system. Freshly installed membranes need a significantly longer time to degas (up to 5 days). After evacuation valves were closed in this sequence, FCV-7, FV-5, FV-8 and lastly FV-13.
4. Valve FV-2 was opened allowing gas to expand up to FCV-7, just prior to the membrane cell.
5. FCV-1 was closed to isolate the working and reference volume from one another.
6. Pressure was reduced within V-100 by applying vacuum using P-100. The rate of evacuation was limited by not fully opening valves FV-3 and FV-6. The pressure was reduced by the amount of pressure drop experienced in V-101 when FCV-7 is opened. When setting the pressure in the reference volume the pressure rise from the compression effect of the next step had to be accounted for.
7. FV-3 was closed, followed by FV-6.
8. P-100 was disengaged to minimize any vibrations.
9. FCV-7 was opened, and the time lag experiment was initiated.

### 2.8 Membrane installation protocol

1. The VCR face seal connection downstream of the membrane was undone using box wrenches.
2. The bolt applying downward pressure on the upper half of the membrane cell was undone, liberating the top half of the membrane cell (downstream side) from the lower half (upstream side).
3. Wearing gloves, the old membrane sample was removed, and vacuum grease was removed from the stainless-steel ring on which membrane samples are seated using isopropyl alcohol and lint free wipes.
4. The Buna-N O-ring gasket was replaced every time the membrane cell was opened, to prevent any leaks that could arise from gasket deformation. The gasket prevents any leaks from the high-pressure side escaping the membrane cell to the atmosphere.
5. Dow Corning High Vacuum Grease was applied on the stainless-steel ring on which the membrane is seated. This vacuum grease helps adhere the membrane in place and acts as a barrier between the low- and high-pressure sides, minimizing gas slipping past the membrane sample.
6. The top half of the membrane cell was put in place and secured using the top bolt.
7. The membrane cell was reconnected to the downstream section, replacing the metal gasket face seal.
8. The system was set to evacuate using the P-401 for multiple days, until degassing could no longer be detected.
9. Leak tests were performed at a high vacuum to ensure the membrane cell is exhibiting an insignificant leak rate.

An external view of the membrane cell can be seen in Figure 6**.**

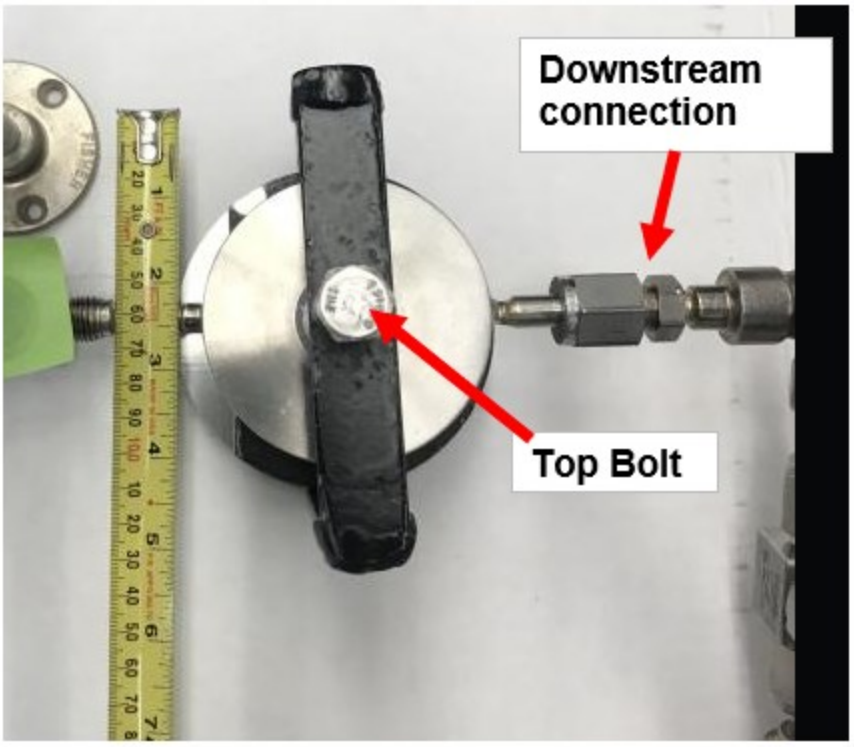


*Figure 6 - Membrane cell.*

## 3.0 Time Lag Contribution of the Downstream Permeate Collector

It has been previously demonstrated [19-20] that the downstream receiver exhibits a resistance to gas accumulation, resulting in a contribution to the measured time lag when characterizing a membrane. The receiver's time lag contribution depends on the configuration (additional volumes, tube diameters and lengths), and is not uniform throughout the receiver [19-20]. Determining the time lag, and transport properties, of membrane samples accurately requires that the receiver's time lag contribution to either be negligible or accounted for post hoc, otherwise over or underestimations of $\theta$, $D$, and $S$ are obtained. In efforts to determine the receiver configuration and measurement location with the lowest magnitude time lag contribution for the apparatus outlined in Chapter 2 a case study was performed. Additionally, the statistical significance of the time lag contribution of the receiver was investigated. A quantitative and qualitative comparison of the receiver's time lag observed to those predicted by the analytical model developed by S. Lashkari and described by Eq. (10)-(15) was performed.

### 3.1 Experimental methodology

High molecular weight polyphenylene oxide (PPO) was dissolved in trichloromethane (MilliporeSigma Canada Ltd, Oakville, Ontario, Canada, 480150) using a magnetic stirrer over 48 h to create a 7.5% w/w PPO solution. The PPO solution was cast on a silicon wafer using a spin coater under vacuum at 150 rpm for 5 minutes. A second layer was cast on top of the first using the same PPO solution at 150 rpm for 5 minutes under vacuum. After spin coating, the silicon wafer backed PPO films were transferred to a vacuum desiccator for 48 h, after which the PPO films were liberated from the wafers by immersion in reverse osmosis water. The PPO films were then dried in between multiple sheets of paper and pressed flat by an 8" concrete block (Home Depot, Kanata, Ontario, Canada, 30169112). The PPO films were left in between the paper for 2 months before being cut into a round disc. The average thickness of the film was 47.5 μm.

A PPO membrane sample was installed in the membrane cell using the procedure outlined in Chapter 2, and all membrane characterization trials were performed as outlined in Chapter 2. The feed gas temperature and pressure were held constant at 303 K and 1600 Torr, respectively. A single PPO membrane sample was utilized for all trials conducted. Nitrogen gas was utilized for all trials. A two-factor experiment with repeated measures was performed so that any interactions or main effects of receiver configuration and the measurement location could be identified. Factor

*A* is the receiver configuration. Four levels of factor *A* were tested ($R_1$-$R_4$). The second factor, factor *B*, is the measurement location, and was tested at two levels using independent absolute pressure transducers, $APT_2$ and $APT_3$, located 0.095 and 0.519 m downstream from the membrane respectively. Both levels of factor *B* were measured simultaneously, for each level of factor *A*. The dependent variable studied is the time lag measured by both APTs and a total of 3 samples per combination of Factors *A* and *B* were observed.

The four levels of factor A are: $R_1$, $R_2$, $R_3$, $R_4$. The receiver configuration $R_1$ consists of only tubing, with the vast majority having a 12.7 mm (½") OD. $R_2$ and $R_3$ are single accumulation tank configurations in which a single tank is added to $R_1$. All additional accumulation tanks are located between $APT_2$ and $APT_3$. $R_2$ utilizes a calibrated $3.0 \times 10^{-4}$ $m^3$ tank located 0.302 m from the membrane whereas $R_3$ uses a $5.0 \times 10^{-4}$ $m^3$ tank located at 0.367 m. A single configuration, $R_4$, was tested utilizing both aforementioned tanks. The experimental apparatus depicted in Figure 7 has a total of three tanks, but no trials were performed utilizing the third tank located at 0.432 m from the membrane as it exhibited a large leak that could not be rectified prior to conducting this study. Table 2 indicates what valves must be opened or closed to achieve configurations, and the corresponding volumes of factor *A* levels $R_1 – R_4$.

*Table 2 – Valve configuration to achieve receiver configurations $R_1$-$R_4$.*

| **Downstream Receiver Configuration** | **Receiver Valves Open** | **Receiver Valves Closed** | **Volume [$m^3$]** |
|---|---|---|---|
| $R_1$ | FV-9 | FV-8,10,11,12,13 | $8.1 \times 10^{-5}$ |
| $R_2$ | FV-9,10 | FV-8,11,12,13 | $3.8 \times 10^{-4}$ |
| $R_3$ | FV-9,11 | FV-8,10,12,13 | $5.8 \times 10^{-4}$ |
| $R_4$ | FV-9,10,11 | FV-8,12,13 | $8.8 \times 10^{-4}$ |

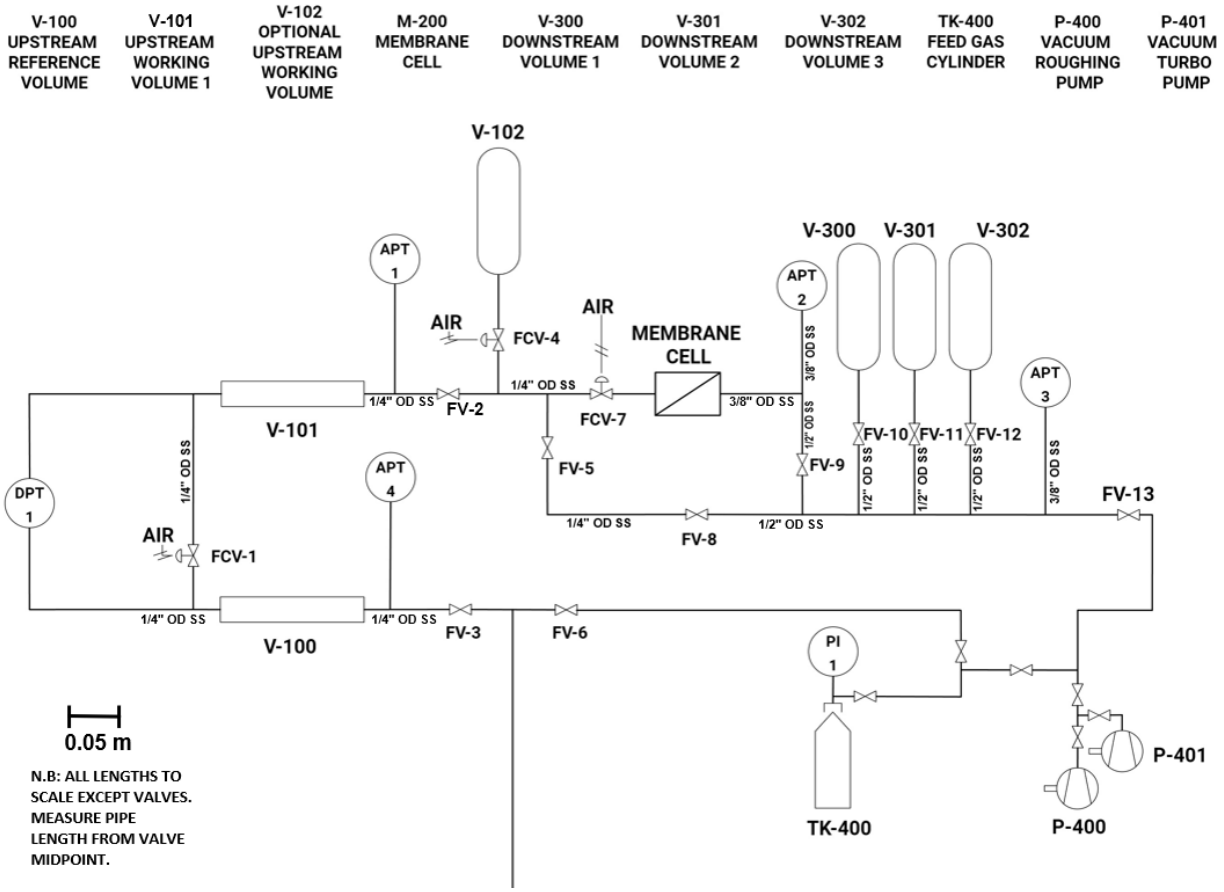


*Figure 7 – Schematic of constant volume system.*

### 3.2 Statistical methodologies

The two-factorial test conducted with $i$=4 levels of factor A, and $j$=2 levels of factor $B$ with $k$=3 repeated measures the independent observations for a given trial may be described by the linear statistical model Eq. (19).

$$Y_{ijk} = \mu + \tau_i + \beta_j + (\tau\beta)_{ij} + \varepsilon_{ijk} \begin{cases} i = 1,2,3,4 \\ j = 1,2 \\ k = 1,2,3 \end{cases} \tag{19}$$

where $\mu$ is the overall mean effect, $\tau_i$ is treatment effect of the $i^{\text{th}}$ level of factor $A$, $\beta_j$ is treatment effect of the $j^{\text{th}}$ level of factor $B$, $(\tau\beta)_{ij}$ is the interaction effect between factor $A$ and $B$ at the $i^{\text{th}}$ and $j^{\text{th}}$ level, and $\varepsilon_{ijk}$ is random error for the $k^{\text{th}}$ repeat measure at the $i^{\text{th}}$ and $j^{\text{th}}$ factor levels.

A two-factor analysis of variance (ANOVA) with repeated measures was performed to determine if factor $A$, or factor $B$ had statistically significant effect on the mean time lag. Since each combination of factors A and $B$ had 3 independent observations the degrees of freedom allow

for the interaction of factors *A* and *B* to be tested. The three null hypotheses being proposed are:

1. The effects of each level of factor *A* on the observed time lag are equal to zero.
2. The effects of each level of factor *B* on the observed time lag are equal to zero.
3. The effect of the interaction between factors *A* and *B* on the observed time lag is equal to zero.

Or symbolically with each respective alternative hypothesis:

$$H_0: \tau_1 = \tau_2 = \tau_3 = \tau_4 = 0$$
$$H_1: \textit{at least one } \tau_i \neq 0 \tag{20}$$

$$H_0: \beta_1 = \beta_2 = \beta_3 = \beta_4 = 0$$
$$H_1: \textit{at least one } \beta_i \neq 0 \tag{21}$$

$$H_0: (\tau\beta)_{11} = (\tau\beta)_{12} \ldots (\tau\beta)_{ij} = (\tau\beta)_{42}$$
$$H_1: \textit{at least one } (\tau\beta)_{ij} \neq 0 \tag{21}$$

The significance level, α, was selected to be 0.01.

### 3.3 Model adequacy

Model adequacy was assessed through the analysis of residuals. The normality of the residuals was examined using quantile normal plot, and homoscedasticity was analyzed by plotting residuals by factor level.

### 3.4 Determination of time lag using downstream pressure rise

Instead of the determining visually with a straight edge when the slope of pressure rise vs time is linear and extrapolating to the x axis to determine time lag, a more analytical approach was employed. A moving window of fixed width was utilized to continuously determine the instantaneous time lag over the course of the trial. A linear regression was found within the bounds of the window from which the x-intercept (time lag) could be extrapolated. A 100 s window was utilized in every analysis, which contained approximately 1700 data points. The window was shifted 1 datum at a time. Figure 8 depicts the moving window method where a linear regression

(solid red line) is extrapolated (dashed red line) to the x-axis.

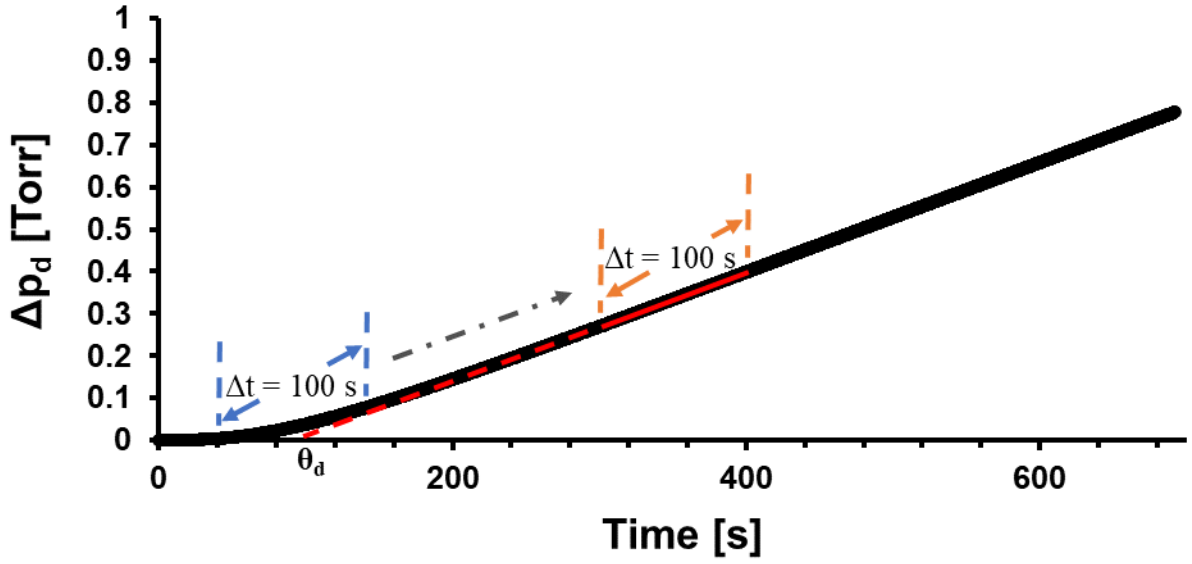


*Figure 8 - Illustration of the moving window analysis on downstream time-lag experiment.*

Plotting the time lag values calculated using the moving window method versus the median time of the moving window yields Figure 9.

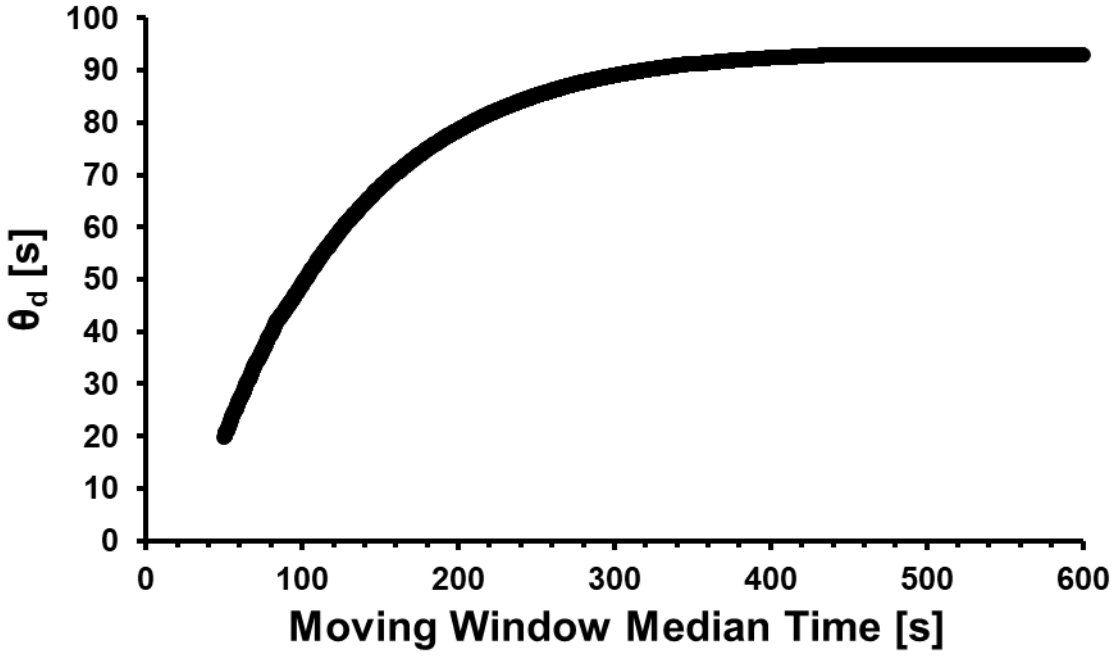


*Figure 9 - Downstream time lag as a function of median moving window time, depicting nitrogen permeating through a PPO membrane with receiver configuration $R_1$ at a pressure of 1600 Torr and 303 K.*

Inspection of Figure 9 shows that a plateau in calculated instantaneous time lag values is reached at around a moving window median time of 400-600 s indicative of a quasi-steady state permeation rate. It was at this plateau, at a median window time of 400 s that $\theta_d$, $P$, $D$ and $S$ were determined. In general, the median window time was varied between different conditions (temperature, pressure, volume), but always corresponded to a plateau in $\theta$ vs $t$, at a time approximately equal to 3–4-time lags, which is in general agreement with when quasi-steady state permeation is achieved when characterizing membranes in CV systems [17].

### 3.5 Results

After collecting the raw data an analysis of residuals was performed to verify the assumptions made when using the general linear model and ANOVA. A plot of the culminative probability vs. residuals showed linear behavior with the exceptions of outliers resulting from data collected during the third repeated measure of time lag for factor A level $R_3$. Disregarding the one significant outlier ($R_3$ Trial 3) a normal distribution of residuals is observed satisfying the assumption made. The residuals were further analyzed by factor levels and equal variance was observed for all factors, except for factor A level $R_3$ where the outlier was observed in the third repeated measure, justifying the assumptions of equal variance made. If more than three repeated measures were performed for each combination of factor and level the deviations from residual normality and equal variance resulting from the outlier would diminish.

Despite one outlier in factor A level $R_3$ a two factor ANOVA with repeated measures was performed including all levels of factor $A$ ($R_3$ was not removed from the data set post hoc). Using significance of $\alpha = 0.01$ the interaction of factors A and B was found statistically significant, in addition to the main effects of both factors, thus all three null hypotheses were rejected. If the same analysis was performed removing factor $A$ level $R_3$ the ANOVA analysis results in the same conclusions, but with an even greater statistical significance. The ANOVA summary table for this studying the effect of receiver configuration and measurement location on the measured time lag is presented in Table 3.

*Table 3 - Two factor ANOVA with repeated measures summary table for determining the statistical significance of the time lag contribution of the downstream receiver.*

| Source of Variation | SS | df | MS | F | P-value | F crit |
|---|---|---|---|---|---|---|
| **Factor A** | 642.98 | 3 | 214.33 | 108.31 | $7.69 \times 10^{-11}$ | 5.29 |
| **Factor B** | 220.59 | 1 | 220.59 | 111.47 | $1.28 \times 10^{-8}$ | 8.53 |
| **Interaction** | 115.81 | 3 | 38.60 | 19.51 | $1.36 \times 10^{-5}$ | 5.29 |
| **Within** | 31.66 | 16 | 1.98 | | | |
| **Total** | 1011.05 | 23 | | | | |

The rejection of the null hypothesis for factors A and B indicates that value of the observed variable, time lag, is dependent on both the receiver configuration, and measurement location. The practical implication of this is that the transport properties of membranes determined using the time lag method in a CV system have an inherent error to them. To accurately determine the transport properties care must be taken in the design of the receiver to minimize the time lag contributions of the receiver, or corrections must be made post hoc. The significance of the interaction between receiver configuration and measurement location implies that the spatial variation of the resistance to gas accumulation within the receiver is affected by the configuration (total volume, and tank locations) utilized. To further investigate the interaction between the two factors a bar plot, Figure 10, was generated showing the mean observed time lag for each factor and level. The same data shown in Figure 10 is provided in Table 1 for reference.

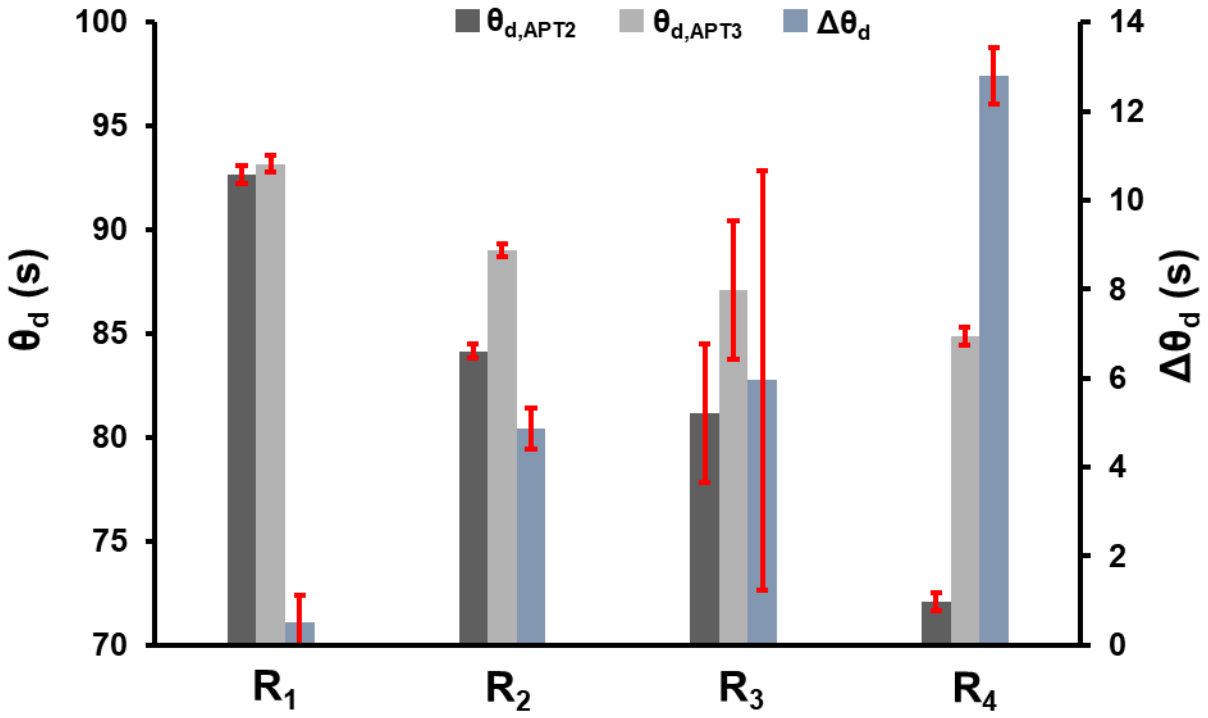


*Figure 10 - Average time lag values for receiver configurations $R_1$-$R_4$. Error bars represent the 95% confidence interval.*

*Table 4 - Mean time lag values for receiver configurations $R_1$-$R_4$.*

| **Downstream Receiver Configuration** | **$\theta_{d,APT2}$ [s]** | **$\theta_{d,APT3}$ [s]** |
|---|---|---|
| **$R_1$** | 92.66 | 93.18 |
| **$R_2$** | 84.15 | 89.01 |
| **$R_3$** | 81.15 | 87.10 |
| **$R_4$** | 72.08 | 84.87 |

Inspection of Figure 10 shows that the difference between the mean time lag values observed by $APT_2$ and $APT_3$ is smallest for receiver configuration $R_1$ and the difference increases as additional volumes are added between the two pressure transducers. The difference of mean time lags increases from 0.52 ± 0.58 s for configuration $R_1$ to 12.79 ±0.63s for configuration $R_4$. Furthermore, it is evident that the measured time lags decrease at both locations as the volume

between $APT_2$ and $APT_3$ increases. Although the time lags at both locations decrease with the addition of accumulation tanks a greater depression is observed at the pressure transducer located closest to the membrane cell before additional volumes ($APT_2$) and a lesser effect is observed by the pressure transducer further from the membrane cell after all additional volumes ($APT_3$).

The receiver's time lag contribution was simulated at the location of $APT_2$ and $APT_3$ for the apparatus outlined by Figure 7 for configurations $R_1 - R_4$ using an analytical model developed by Lashkari described by Eqs. (10)-(15) [20]. The results of the simulated time lag contributions and differences between both time lags are presented in Table 5 alongside the experimentally observed differences.

*Table 5 - Predicted receiver time lag contributions for configurations $R_1$-$R_4$ and the experimentally observed time lag differential between $APT_3$ and $APT_2$.*

| Downstream Receiver Configuration | Simulated | | | Experimental |
|---|---|---|---|---|
| | $\theta_{d,APT2}$ [s] | $\theta_{d,APT3}$ [s] | $\Delta\theta_d$ [s] | $\Delta\theta_d$ [s] |
| $R_1$ | -0.09 | 0.04 | 0.13 | 0.52 ± 0.58 |
| $R_2$ | -1.21 | -0.60 | 0.60 | 4.86 ± 0.47 |
| $R_3$ | -2.32 | -1.16 | 1.16 | 5.94 ± 4.72 |
| $R_4$ | -2.66 | -1.04 | 1.63 | 12.79 ± 0.63 |

### 3.6 Discussion

#### 3.6.1 Receiver configuration $R_1$

The simplest permeate receiver configuration $R_1$ comprised of mostly 12.7 mm (½") OD tubing with no additional volumes was predicted to have a time lag contribution of -0.09 and 0.04 s at the locations of $APT_2$ and $APT_3$ respectively. The low resistance to gas accumulation of configuration $R_1$ is a result of following the design heuristics proposed by Lashkari [20], utilizing ½" OD tubing for the main line, and limiting the length of the main line, in this case to 0.602 m. Upon initiating the time lag experiment, the receiver is under a high vacuum, $6.5 \times 10^{-4}$ Pa or less, and conditions for Knudsen diffusion exist within the 12.7 mm (½") tubing. Since the Knudsen diffusion coefficient is directly proportional to the tube diameter, the diffusion coefficient (1.63

$m^2/s$ for $N_2$ at 303.15 K in 12.7 mm tubing) was maximized given the options of tubing sizes available for the receiver of the CV system at the time of construction. Furthermore, as gas accumulates in the receiver, the pressure rises, and the mean free path of molecules decreases. The larger the diameter tube, the lower pressure is required for the criterion of $r/\lambda < 0.1$, for which Knudsen flow is applicable, is exceeded and the resistance to the flow of gas within the receiver decreases. For where the receiver is a single tube, as Eq. (9) indicates, both the maximum positive and negative time lag contribution of the receiver is directly proportional to the square of the overall length of the main line $Z_n$. Had a shorter length of tube been used in the design of the receiver the magnitude of the positive and negative time lag contribution could be further reduced.

Since the observed time lag is a combination of both the time lag of the membrane, and the receiver, the receiver's contribution could not be directly measured using the experimental methodology outlined in this chapter. To measure the time lag contribution of the receiver directly, gas permeating through the membrane would need to be replaced with a source of constant flowrate with no resistance, such as gas fed by a mass flow controller. However, by taking the difference between the observed time lag measured by $APT_3$ and $APT_2$, the time lag contribution of the membrane is removed, and the resulting time lag differential can be attributed to the receiver alone. The difference of the time lags measured by $APT_3$ and $APT_2$ can be compared to those predicted in Table 5. The time lag differential predicted for receiver configuration $R_1$ is the same order of magnitude as the observed differential and falls within the 95% confidence interval.

Although the time lag differential between $APT_3$ and $APT_2$ is two orders of magnitude lower than the observed time lag for the trials conducted using $R_1$, it does not definitively prove the time lag contribution of the receiver is negligible in this configuration. A receiver could be designed with a large time lag contribution, but equal in magnitude at both locations where data sampling occurs, which would result in the same phenomena of equal observed time lags for the membrane being characterized.

### 3.6.2 Receiver configurations $R_2$, $R_3$, $R_4$

The predicted time lag contributions, seen in Table 5, for receiver configurations $R_2$, $R_3$, and $R_4$ at the locations corresponding to $APT_2$ and $APT_3$ are negative, and are expected to decrease the magnitude of the measured time lag of the PPO sample being characterized. The analytical model for the receiver predicts that the depression of time lag values measured by $APT_2$ increases

in magnitude, as the volumes downstream of $APT_2$ increases, referencing Figure 10 this trend was observed experimentally. Although the trend of decreased time lags measured by $APT_2$ was like that predicted, the magnitude of the depression observed experimentally was greater than predicted. A similar phenomenon was observed by Lashkari et al. [19] where the observed time lag depression was greater than predicted.

For configurations $R_1$–$R_3$ the time lag depression observed by $APT_3$, the pressure transducer down stream of all additional volumes, was not as large as those observed by $APT_2$, as predicted by the analytical model. This corresponds to analysis of a model for a single tank receiver developed by Lashkari et al. [20] where measurements made closer to the flow source, prior to the additional volume, experiences a large time lag depression, with a lesser effect on measurements made downstream of the additional volumes. The inequality of time lag depression at both locations causes an increase in time lag differential observed as larger volumes are added in between both APTs. Similarly, to $APT_2$ the time lag depression observed by $APT_3$ is greater in magnitude than predicted.

### 3.7 Conclusion

Although it was not proven, it is concluded that the time lag contribution of receiver configuration $R_1$ is negligible and should be used to establish a benchmark time lag value for those determined by upstream pressure decay tests in Chapter 5. The motivation for this assumption is that the predicted time lag contributions of $R_1$ is three orders of magnitude lower than the measured time lag for the PPO membrane sample characterized. Furthermore, the measured time lag differential between $APT_3$ and $APT_2$ was like that predicted using the analytical models providing some evidence that the model closely describes reality for configuration $R_1$. $APT_3$ should be utilized for membrane characterization in any configuration as of the two possible locations it experiences a lesser magnitude contribution from the receiver.

The transport properties, $P$, $S$, $D$, were calculated from the pressure rise vs time data collected using $APT_2$ and $APT_3$ for configurations $R_1$-$R_4$ and presented in Table 6 along with the error relative to those calculated using data collected by $APT_3$ with configuration $R_1$.

*Table 6 - Transport properties P, D, and S determined using receiver configurations $R_1$-$R_4$ and the relative errors with respect to $R_1$ $APT_3$.*

| Downstream Receiver Configuration | Transport Properties | | | Relative Error | | |
|---|---|---|---|---|---|---|
| | P | S | D | P | S | D |
| | [$m^3$(STP)•m/$m^2$/Pa/s] | [mol/$m^3$/Pa] | [$m^2$/s] | % | % | % |
| | | | $APT_2$ | | | |
| $R_1$ | $2.38x10^{-17}$ | $2.66x10^{-4}$ | $4.07x10^{-12}$ | 1.42 | 0.85 | 0.56 |
| $R_2$ | $2.39x10^{-17}$ | $2.43x10^{-4}$ | $4.48x10^{-12}$ | 1.92 | -7.95 | 10.73 |
| $R_3$ | $2.40x10^{-17}$ | $2.35x10^{-4}$ | $4.65x10^{-12}$ | 2.32 | -10.90 | 14.96 |
| $R_4$ | $2.43x10^{-17}$ | $2.11x10^{-4}$ | $5.23x10^{-12}$ | 3.50 | -19.93 | 29.27 |
| | | | $APT_3$ | | | |
| $R_1$ | $2.34x10^{-17}$ | $2.64x10^{-4}$ | $4.04x10^{-12}$ | 0.00 | 0.00 | 0.00 |
| $R_2$ | $2.36x10^{-17}$ | $2.53x10^{-4}$ | $4.23x10^{-12}$ | 0.58 | -3.91 | 4.68 |
| $R_3$ | $2.37x10^{-17}$ | $2.49x10^{-4}$ | $4.33x10^{-12}$ | 1.20 | -5.41 | 7.01 |
| $R_4$ | $2.39x10^{-17}$ | $2.45x10^{-4}$ | $4.44x10^{-12}$ | 1.91 | -7.17 | 9.78 |

Comparing the relative errors between the possible configurations and measurement locations it is evident that the time lag contribution of the receiver has the greatest effect on the *D*, which were overestimated anywhere from 0.56% to 29.27% depending on the pressure transducer and configuration used. Underestimations of time lag results in overestimations of *D*, which results in an underestimation of *S*, as *P* was found to vary minutely between receiver configuration and sampling location. This resistance to gas accumulation within the receiver having less pronounced effect on *P* in comparison to *S,* and *D,* is consistent with previous observations [20].

Ideally the time lag contribution of the receiver should be measured directly using a mass flow controller in place of gas permeating through a membrane. This measurement could be used post hoc to correct time lag measurements done with membrane samples. If such a calibration is performed, care should be taken as to match the flow rate of gas as would be achieved with the membrane sample being characterized, as to not stay in, or prematurely depart from the Knudsen flow regime, as this would result in an incorrect time lag correction.

## 4.0 Determination of the Activation Energy of Permeation, Diffusion, and Enthalpy of Solution Using the Downstream Time-Lag Method

The temperature dependence of permeation, diffusion, and solution of gas within a polymeric membrane have been shown to follow the three Arrhenius type relations described by Eq. (22)-(24) [10].

$$P = P_0 e^{\frac{-E_P}{RT}} \tag{22}$$

$$D = D_0 e^{\frac{-E_D}{RT}} \tag{23}$$

$$S = S_0 e^{\frac{-\Delta H_S}{RT}} \tag{24}$$

By determining $P$, $D$, and $S$ at various temperatures a plot of the natural logarithm as a function of inverse temperature allows determination of the activation energies of permeation ($E_P$), diffusion ($E_D$), and the enthalpy of solution ($\Delta H_S$).

### 4.1 Experimental methodology

A PPO membrane sample was previously installed in the membrane cell of the CV system using the procedure outlined in Chapter 2, and all trials were conducted using the protocol outlined in Chapter 2. The details of the CV system used are provided in Figure 2.

A series of two one-factor experiments was performed, where the independent factor $C$, corresponding to the gas feed temperature, was tested at four levels ranging from 275–303 K. Three repeated measurements were performed for every level of factor $C$. Pressure was held constant at 1800 Torr between all trials, and a singular PPO sample was utilized. Downstream receiver configuration $R_1$ comprised of mostly 12.7 mm (½") tubing and no additional volumes was used. The observed variable, pressure within the downstream receiver, was monitored using $APT_3$.

As the CV system is located within an insulated enclosure the independent variable, $T$, was manipulated by adjusted the temperature of the air bath within the enclosure. The ambient temperature of the lab which the enclosure is located within varied from 293-296 K, thus this temperature range was not tested as temperature control was achieved using either heating or cooling functions exhibited in Chapter 2. Temperatures above ambient were maintained within ±0.05 K, whereas sub ambient temperatures could only be maintained within a range of ±0.6 K

due to the limitations of the cooling functionality outlined in Chapter 2. Gas temperatures within the CV system could not be directly measured and was assumed to be the average temperature range of the air bath within the enclosure.

A total of two pure gas species namely, nitrogen, and oxygen were tested. All factor levels were tested and repeated measurements were taken using a nitrogen feed before switching to oxygen. When switching the feed gas to oxygen the entirety of the CV system (upstream and downstream of the membrane) was filled with oxygen and evacuated ten times to flush out the bulk of nitrogen gas present in the system. After the series of flushes was performed, the entire CV system was allowed to fully degas by applying a high vacuum until degassing from the membrane/tube walls could no longer be detected.

### 4.2 Determination of time lag and transport properties

The downstream time lag, $\theta_d$ was determined using the moving window methodology outlined in Chapter 3. Assuming the applicability of Henry's law, the transport properties $P$, $D$ and $S$ were determined as outlined in Chapter 1.

### 4.3 Determination of the activation energies, enthalpy of solution and preexponential constants

Linearization of Eqs. (22)-(24) allows for the determination of the activation energies and preexponential coefficients for $P$, $D$, and $S$ through linear regression. Additionally linear regression allows for the statistical significance of the results, and the applicability of the Arrhenius equation over the temperature range tested to be evaluated. Linearization of Eqs. (22)-(24) results in Eqs. (25)-(27).

$$\ln(P) = \ln(P_0) + \frac{-E_P}{RT}\frac{1}{T} \tag{25}$$

$$\ln(D) = \ln\left(D_0\right) + \frac{-E_D}{RT}\frac{1}{T} \tag{26}$$

$$\ln(S) = \ln\left(S_0\right) + \frac{-\Delta H_S}{RT}\frac{1}{T} \tag{27}$$

Three identical sets of null hypotheses tested are:

1. The independent variable ($1/T$) has no effect on the dependent variable (the natural logarithm of $P$, $S$ or $D$), i.e., the slope of $\ln(P)$, $\ln(S)$ and $\ln(D)$ vs $1/T$ is equal to zero.
2. The y-intercept is equal to zero.

With the alternative hypotheses:

1. The independent variable ($1/T$) affects the dependent variable (the natural logarithm of $P$, $S$ or $D$), i.e., the slope of $\ln(P)$, $\ln(S)$ and $\ln(D)$ vs $1/T$ not equal to zero.
2. The y-intercept is not equal to zero.

To determine the statistical significance a two tailed t-test was performed with a significance level of $\alpha=0.01$ for each proposed hypothesis.

### 4.4 Linear regression model adequacy

The assumptions made to perform a linear regression analysis were validated through an analysis of the residuals. The normality of the residuals was examined using quantile normal plot, and homoscedasticity was analyzed by plotting residuals by factor level. Plots of $\ln(P)$, $\ln(D)$, and $\ln(S)$ vs $1/T$ were generated to verify the linearity assumption made between the dependent and independent variables.

#### 4.4.1 Model adequacy

Analysis of the quantile-normal plots of the residuals for the three linear regressions performed yielded a linear relation indicating that the residuals follow a normal distribution, satisfying the assumption made. When checking for homoscedasticity it was noticed that the equal variance assumption was not fully justified. When residuals were grouped by level of factor $C$ (temperature), equal variance was only observed between trials performed below ambient temperatures, but a much smaller variance was observed when operating above ambient conditions. The unequal variance stems from the fact that when operating below ambient temperatures the fluctuations in temperature within the enclosure housing the CV system were an order of magnitude greater than when heating was used. Despite one level of factor A exhibiting a much smaller variance than the other three factors the linear regression analysis was deemed to be

suitable as moderate violations of equal variance tend to cause minimal problems when utilizing a linear regression analysis [28].

Plots of ln($D$), ln($P$), and ln($S$), vs. 1/$T$ illustrated by Figure 11 - Figure 13 show that assumption of linearity is upheld, and that a linear regression analysis can be utilized.

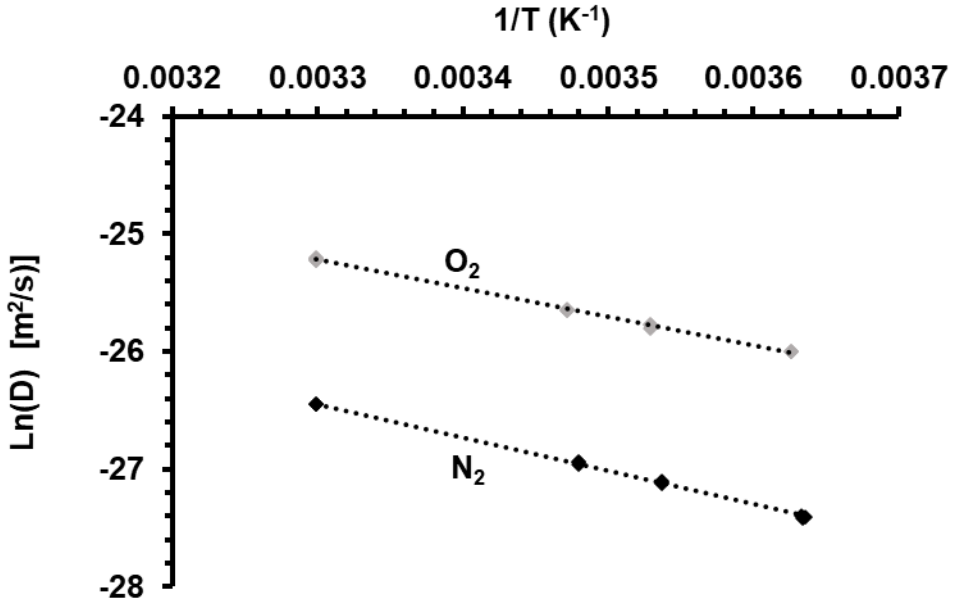


*Figure 11 - Natural logarithm of diffusivity versus inverse temperature.*

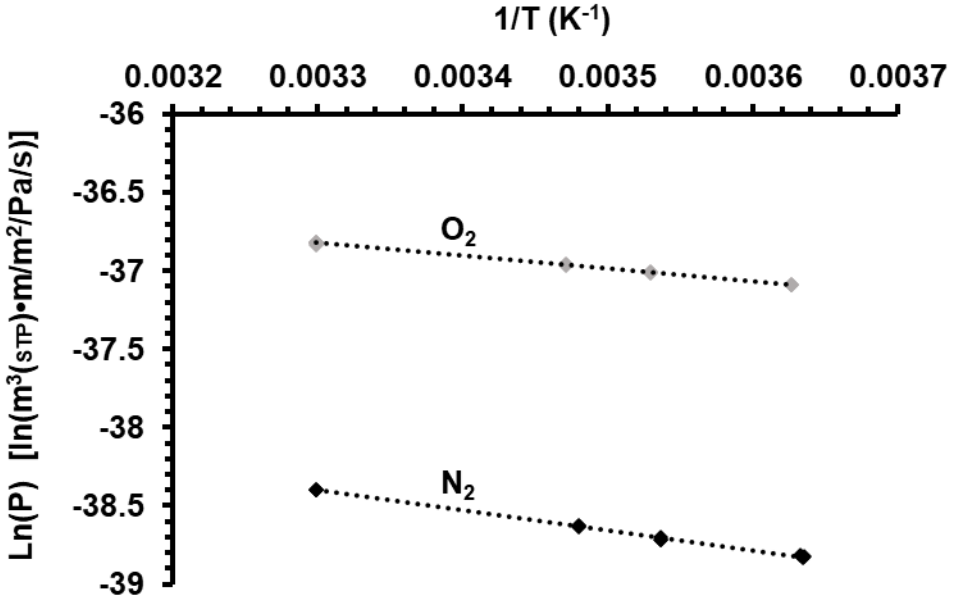


*Figure 12 - Natural logarithm of permeability versus inverse temperature.*

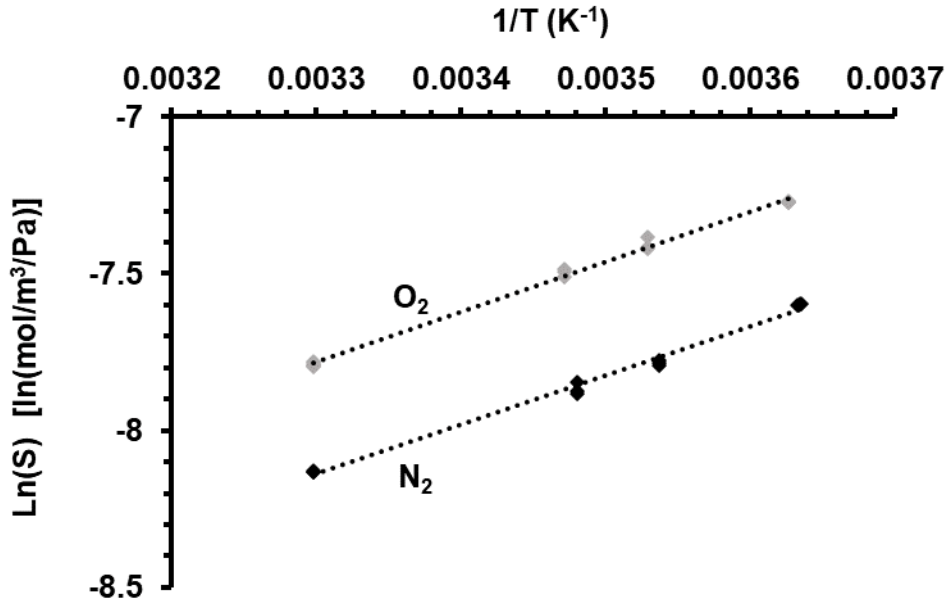


*Figure 13 - Natural logarithm of solubility versus inverse temperature.*

P-values determined for each parameter are orders of magnitude below the significance level of $\alpha$=0.01, thus all null hypotheses were rejected, and it was concluded that ln(*P*), ln(*D*), and ln(*S*) are all a function of 1/*T* and that the y-intercepts are none zero. This indicates that the findings presented are statistically significant and likely not a result of random error. The coefficient of determination, $R^2$, for all 6 linear regressions yielded a value greater than 0.99 indicating the measured variability of *P*, *D*, and *S* as a function of temperature are explained by an Arrhenius type law at constant a constant pressure over the examined temperature range.

### 4.5 Activation energy of permeation, diffusion, and enthalpy of solution

The constant pressure activation energies of permeation, diffusion, and heats of solution for oxygen, and nitrogen, within PPO are provided in Table 7, alongside the preexponential factors for Arrhenius type relations Eqs. 22-24.

*Table 7 - Activation energy of permeation, diffusion, and enthalpy of solution and associated preexponential factors for oxygen and nitrogen gas within a PPO membrane.*

| Gas | $P_0$ [$m^3$(STP)/$m^2$/Pa/s] | $E_p$ [kJ/mol] | $D_0$ [$m^2$/s] | $E_d$ [kJ/mol] | $S_0$ [mol/$m^3$/Pa] | $\Delta H_s$ [kJ/mol] |
|---|---|---|---|---|---|---|
| $O_2$ | $1.48x10^{-15}$ | 6.75 | $3.24x10^{-8}$ | 20.10 | $2.08x10^{-6}$ | -13.35 |
| $N_2$ | $1.43x10^{-15}$ | 10.63 | $3.88x10^{-8}$ | 23.64 | $1.67x10^{-6}$ | -13.01 |

Table 8 provides the mean value of *P*, *D*, and *S* measured using the downstream time lag at the four temperatures tested.

*Table 8 - Transport properties and permselectivity of oxygen and nitrogen gas for a PPO membrane.*

| T [K] | Gas | P [$m^3$(STP)/$m^2$/Pa/s] | D [$m^2$/s] | S [mol/$m^3$/Pa] | $P_{O_2}/P_{N_2}$ |
|---|---|---|---|---|---|
| 303.15 | $O_2$ | 1.02E-16 | 1.13E-11 | 4.13E-04 | 4.85 |
| | $N_2$ | 2.11E-17 | 3.26E-12 | 2.94E-04 | |
| 287.35 | $O_2$ | 8.87E-17 | 7.28E-12 | 5.54E-04 | 5.32 |
| | $N_2$ | 1.67E-17 | 1.98E-12 | 3.83E-04 | |
| 282.75 | $O_2$ | 8.45E-17 | 6.33E-12 | 6.07E-04 | 5.49 |
| | $N_2$ | 1.54E-17 | 1.68E-12 | 4.17E-04 | |
| 275.15 | $O_2$ | 7.81E-17 | 5.11E-12 | 6.95E-04 | 5.66 |
| | $N_2$ | 1.38E-17 | 1.25E-12 | 5.01E-04 | |

The heats of solution for oxygen and nitrogen in PPO were both determined to be negative, indicating an exothermic process, meaning that temperature and solubility are negatively correlated. This means that the positive correlation of temperature and permeability observed can only be attributed to the increased diffusivities at elevated temperatures. The ideal permselectivity of oxygen and nitrogen was found to decrease with temperature, ranging from 5.66 to 4.85.

### 4.6 Discussion of results

The activation energies for permeation and diffusion and enthalpies of solutions determined and presented in Table 7 are generally consistent with those found in literature reported for gas/polymer systems [10,29]. The values determined in this work are reported again in Table 9 alongside the values reported by Haraya et al. [29].

*Table 9 - Activation energy of permeation, diffusion, and enthalpy of solution for oxygen and nitrogen gas within a PPO membrane. Values from [29] converted from cal/mol to kJ/mol.*

| Gas | $E_P$ [kJ/mol] | $E_D$ [kJ/mol] | $\Delta H_S$ [kJ/mol] | Ref. |
|---|---|---|---|---|
| **$O_2$** | 6.75 | 20.10 | -13.35 | - |
| **$N_2$** | 10.63 | 23.64 | -13.01 | - |
| **$O_2$** | 6.82 | 22.80 | -15.98 | [29] |
| **$N_2$** | 10.21 | 29.37 | -19.16 | [29] |

The activation energy of permeation reported by Haraya [29] for oxygen and nitrogen differs by approximately 1 and -4 % respectively relative to the values measured in this work. The largest discrepancy arises from the activation energy of diffusion and enthalpy of solution, with up to a 47 % relative error on the enthalpy of solution of nitrogen in PPO. Initially it was suspected that the source of the discrepancy between the activation energies of diffusion and heats of solution could arise from the measurements being performed at different pressures. As PPO is a glassy polymer, the applicability of Henry's law is questionable, and the transport properties, and thus activation energies and heats of solution are only applicable locally at the pressures tested [29]. Comparing the experimental methodologies, both measurements were performed at approximately the same pressures. Although the pressure at which the PPO characterization trials were performed by Haraya were not explicitly reported, it was mentioned that a 760-1520 Torr pressure differential was used between the high- and low-pressure side of the membrane, with the low-pressure side being at vacuum conditions [29]. Similarly, PPO was characterized at a pressure of 1600 Torr within this work. Further comparison between the two experimental methodologies shows that the observed time lag values by Haraya varied by 3% for $P$, but a greater discrepancy of up to 15% was observed for $\theta_d$ [29]. Error on $P$ and $\theta_d$ measured using the experimental methodology, and CV system presented in Chapter 2, yielded a significantly smaller relative error of being approximately 3 % for $\theta_d$, and less than 1% for $P$. Alternative explanations for the discrepancies in the heats of solution and activation energy of diffusion could arise from the resistance to gas accumulation within the downstream receiver. Had a receiver been used with a significant time lag contribution to the measured time lag, and consequently by relation of Eq. (1) and Eq. (2), the values of $D$ and $S$ would be affected significantly. As observed experimentally in Chapter 3,

receiver time lag contributions play a lesser role in the measured value of $P$, than $S$ and $D$, possibly explaining why the values of $E_P$ are in better agreeance than $E_D$ and $\Delta H_S$. Other factors may also include the effect of physical aging of the membranes, and different sources of PPO used to manufacture the membrane.

## 5.0 Time Lag Experiment Utilizing Pressure Decay

The initial conditions present in the upstream volume when characterizing a membrane using upstream pressure decay are such that the working volume is set to the feed pressure at which the membrane transport properties are to be determined. The membrane cell and downstream receiver sections of the CV system had been evacuated until all the gas from the previous trial desorbed and equilibrium at vacuum pressures was established. Upon initiation of the time lag experiment a valve isolating the working volume from the membrane cell is opened, and a step-change in pressure within the membrane cell initiating the time lag experiment.

There is a dead volume within the upstream section of the membrane cell bounded by the isolation valve, and the membrane face, that is initially at vacuum prior to the step change in pressure occurring. Gas expanding into the dead volume of the membrane cell causes a rapid pressure drop in the working volume. As gas enters the membrane cell, it sorbs onto the surfaces of the membrane cell and the membrane sample. Simultaneously, gas permeates through the membrane from the high to low pressure side. The initial pressure drop resulting from gas expansion is a near instantaneous process, while gas adsorption and permeation occur over an extended period, causing in the decay of pressure within the working volume over the duration of the upstream time lag experiment.

Assuming a constant temperature, and negligible leak rates, the total pressure decay at time $t$ during a membrane characterization trial can be represented by Eq. (28).

$$\Delta p_u(t) = \Delta p_{u,E} + \Delta p_{u,A}(t) + \Delta p_{u,P}(t) \tag{28}$$

where $\Delta p_u(t)$ is the total upstream pressure drop within the working volume at time $t$, $\Delta p_{u,A}(t)$ and $\Delta p_{u,P}(t)$ is the pressure drop within the working volume caused by gas adsorption on the membrane cell surfaces, and gas permeating through the membrane from time $t$=0 to $t$ respectively.

To utilize the high resolution of a DPT, prior to initiating a membrane characterization trial, the pressure in the reference volume must be reduced to the pressure anticipated in the working volume after gas expansion, as the magnitude of the pressure drop within even a relatively small dead volume would result in the DPT being out of range (±1.0 Torr). This was achieved by employing the experimental procedure outlined in Chapter 2. Due to the large initial pressure differential between the working and reference volumes, the DPT cannot be utilized to measure the pressure differential prior to initiating the time lag experiment. Thus, the initial pressure differential between both volumes ($\Delta p_i$) must be found using the two upstream absolute pressure

transducers as shown in Eq. (29).

$$\Delta p_i = p_{APT_{1,t=0}} - p_{APT_{4,t=0}} \tag{29}$$

where $p_{APT_{1,t=0}}$, and $p_{APT_{4,t=0}}$ is the pressure measured by the upstream absolute pressure transducer at $t$=0 in the working, and reference volume respectively. Assuming an appropriate pressure differential between the upstream volumes was set prior, after initiating the time lag experiment the pressure within the working volume will rapidly decrease within the range of the DPT allowing for the direct measurement of the pressure differential between both volumes ($\Delta p_t$) with a high resolution.

$$\Delta p_t = \Delta p_{DPT,t} \tag{30}$$

where $\Delta p_{DPT}$ is the pressure differential measured by the DPT at $t$=t. Due to the range limitations of the DPT the plot of the total upstream pressure decay from $t$=0 s to test completion can be generated using the piecewise function outlined by Eq. (31).

$$\Delta p_u(t) = \begin{cases} \Delta p_i - \Delta p_i = 0 & for\ t = 0 \\ \Delta p_t - \Delta p_i & for\ t > 0 \end{cases} \tag{31}$$

## 5.1 The zero problem

Figure 14 depicts the measured pressure decay curve, generated using Eq. (31), during an upstream time lag experiment. It can be seen in Figure 14 that initially the expansion of gas into the dead volume causes a pressure drop that is much greater in magnitude than the pressure drop resulting from gas adsorption and permeation.

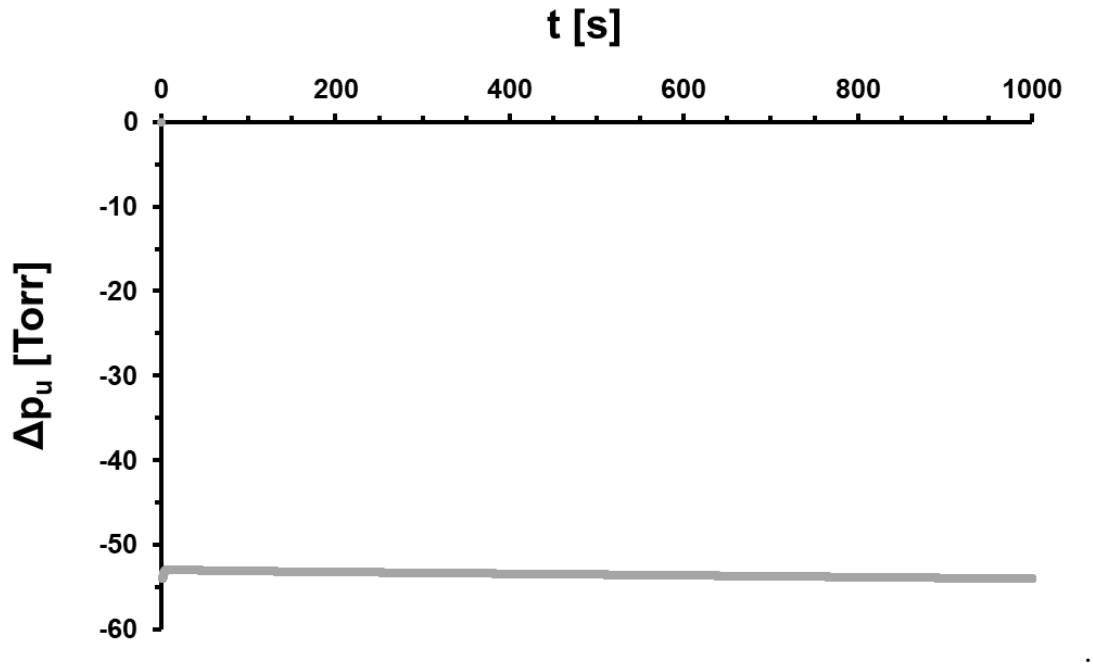


*Figure 14 - Pressure decay response for nitrogen at a feed pressure of 1798 Torr at 303 K permeating through a PPO membrane with no zero correction.*

Accounting for the pressure drop resulting from gas expansion and adsorption is essential for accurate determination of transport properties utilizing upstream pressure decay and the time-lag method. The additional pressure drop from gas expansion shifts the pressure decay curve down the y-axis to a more negative value, thus shifting the x-intercept extrapolated from the linear section of the decay curve. This has the effect of increasing the magnitude of the upstream time lag. For the example, depicted in Figure 14 if the decay curve is not adjusted, the upstream time lag is found to be -52,000 s, approximately 448 times greater in magnitude than $\theta_d$ that was measured to be 116 s for the same trial. Assuming the applicability of Henry's law and ideal boundary conditions for the time-lag method, the expected ratio of $\theta_u/\theta_d$ is expected to be -2 as seen by dividing Eq. (16) by Eq. (1). This large discrepancy motivates the need for the measured pressure decay curve to be adjusted to account for any pressure drop that is not directly a result of gas permeating through the membrane into the downstream receiver.

### 5.1.1 Zero correction – Methodology 1

The first methodology employed to determine the true origin of the pressure decay curve resulting from solely gas permeation was to measure the pressure drop from expansion, and

adsorption ($\Delta p_{u,AE}(t)$) experimentally during a 'calibration run' and directly subtract the result from a decay curve generated from data collected during a membrane characterization trial. The rational for this methodology is that all variables (feed temperature, pressure, gas composition, reference volume, and dead volume) are kept constant, and by replacing the permeable membrane with an impermeable barrier material the leftmost term in Eq. (28) is eliminated resulting in Eq. (32). By taking the difference between Eq. (32) and Eq. (28) we can isolate the pressure decay from permeation resulting in Eq. (33).

$$\Delta p_{u,AE}(t) = \Delta p_{u,E} + \Delta p_{u,A}(t) \tag{32}$$

$$\Delta p_{u,P}(t) = \Delta p_u(t) - \Delta p_{u,AE}(t) \tag{33}$$

By using the same experimental procedure outlined in Chapter 2 and replacing the permeable PPO membrane with an impermeable barrier material, a calibration curve was generated using Eq. (31). The impermeable barrier material selected for this calibration curve was copper shim stock. Shim stock was utilized as it could be purchased in the appropriate thickness where it would not inhibit the membrane cell from forming a tight seal, minimizing leaks. Copper was chosen as it was softer than the stainless-steel ring on which the membrane/copper shim stock is seated, allowing it to be compressed forming a tight seal like a metal gasket, thereby minimizing leaks across the membrane cell from the high pressure to the low-pressure side. When creating calibration curves the same feed pressure, temperature, and composition was utilized as the membrane characterization trial to which it was applied.

Figure 15 shows a plot of the measured upstream pressure decay curves for the calibration run utilizing the impermeable barrier material, and two PPO membrane characterization trials using nitrogen gas at a feed pressure of 1798 Torr at 303 K. The scale of the y-axis was selected such that the general shape of the curves could be seen, but it should be noted that each measurement includes the origin. Inspection of Figure 15 shows that the initial pressure drop from gas expansion for both membrane characterization trials and the calibration curve are similar, leading to an initial pressure drop ranging from 52.8-52.9 Torr. The blue curve in Figure 15 depicting the calibration curve experiences a more gradual pressure decay in comparison to the membrane characterization trials. The lesser magnitude of the calibration run's slope was expected, as it should only be a measure of the rate of adsorption, in comparison to the trials utilizing a membrane where permeation also occurs.

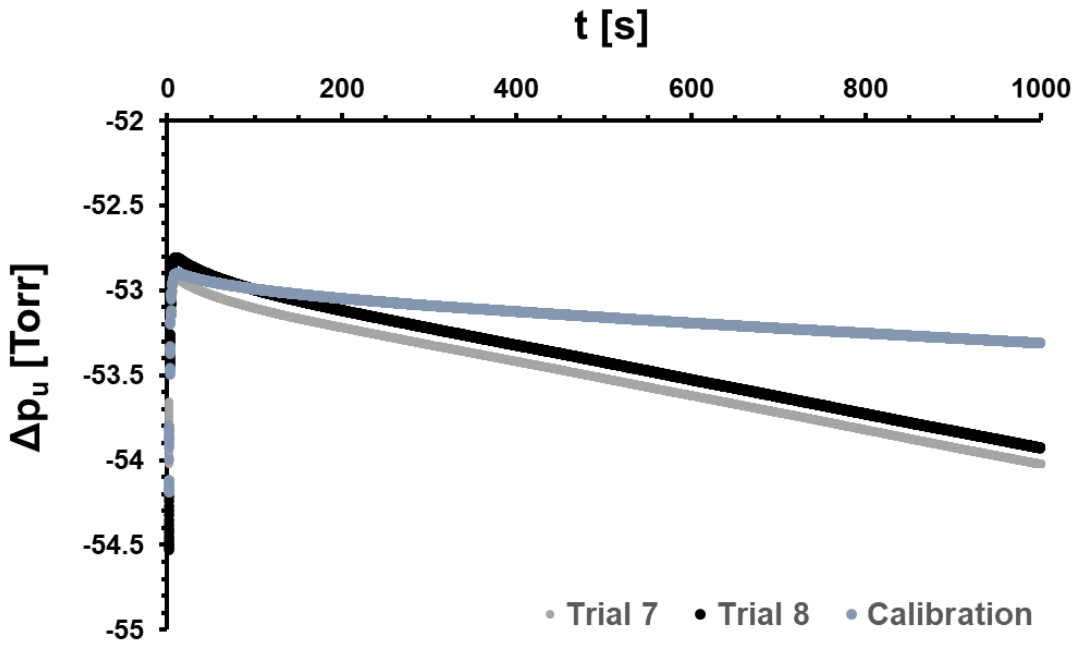


*Figure 15 - Pressure decay curves for two gas permeation trials (black and grey), and one calibration run (blue) using nitrogen at 1798 Torr and 303 K.*

By applying Eq. (30) the upstream pressure decay curves measuring only nitrogen permeating through the PPO membrane were generated resulting in Figure 16.

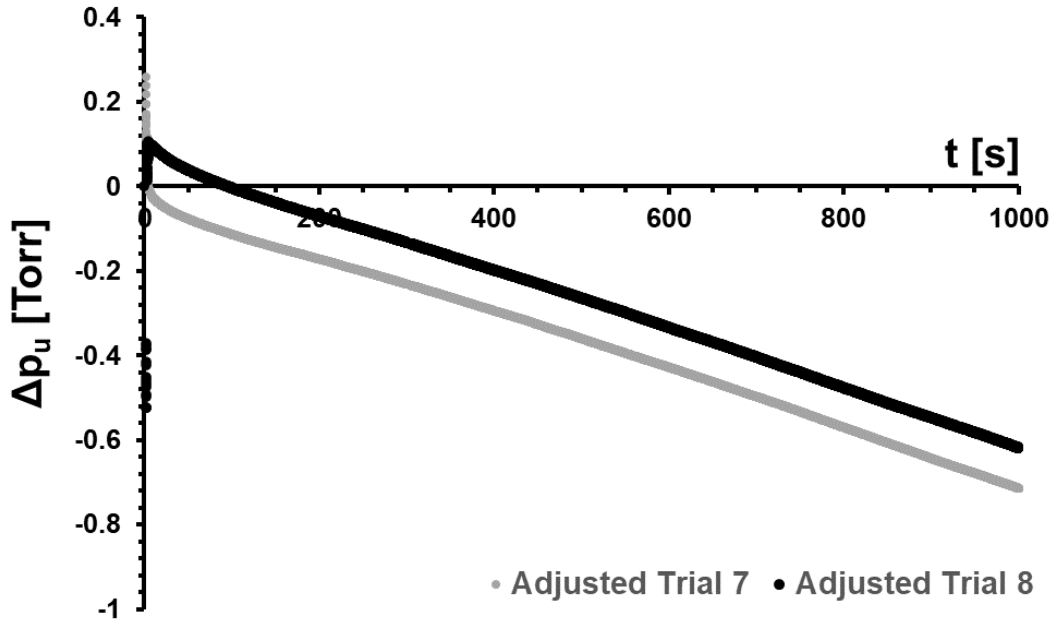


*Figure 16 - Adjusted Pressure decay curves for two PPO membrane characterization trials (black and grey) using Nitrogen at 1798 Torr and 303 K.*

The adjusted pressure decay curves pictured in Figure 16 more similarly represent a decay curve resulting from gas permeating through a PPO membrane in comparison to the decay curve seen in Figure 14. Closer inspection of Figure 16 reveals that descrepencies still exist. The first and most apparent issue is that although both tests were performed at similar conditions the two decay curves from the independent trials do not overlap. The upstream time lag found from the adjusted pressure decay curves for Trials 6 and 7 seen in Figure 16 is -78.5 and 94.5 s respectivly. The time upstream time lag values found from both the adjusted pressure decay are not physically possible, as the upstream time lag should always be both negative and greater in magnitude then than the downstream time lag, which was found to be 115.68 and 115.65 s respectively.

The decay curves for the calibration run, and membrane characterization trials were generated using Eq. (31), which required the initial pressure differential between working and reference volume to be detemined using the high pressure (2000 Torr) absolute pressure transducers. The pressure transuducers utilized on the high pressure side have a resolution of $10x10^{-5}$ of the full scale, which corresponds to 0.02 Torr. As the difference between $APT_4$ and $APT_1$ is taken the error propgates and increases in magnitude, and when inspecting Figure 16, it can be seen that the two decay curves are only shifted along the y-axis by approximately 0.1 Torr, thus the resolution error is not neglegible for correction methodolgy 1.

The effect of the working, or reference volume pressure not being exactly the same between the calibration run and the membrane characterization trial was also considered. As described in Chapter 2, the pressure of the working volume and reference volume was set through the use of hand operated valves, and was subject to some variability (±0.1 Torr) between trials. However, assuming that the pressure drop from gas expansion is constant between the calibration and characterization trials, these errors in intital working and reference volume pressures would simply mean either $\Delta p_t$ or $\Delta p_i$ in Eq. (31) would be greater, and the other would be lesser, by the same amount netting a difference of zero between the two decay curves. Knowing the upstream volumes the assumption of constant pressure drop due to gas expansion was verified with the ideal gas law. If pressures within the working volume varried by 0.1 Torr between trials, the expected change in the pressure drop between would equate to 0.006 Torr, much less than the errors that could be caused by the resolution error of the pressure transducers. As a result of this analysis it was concluded that this type of error was likley not the cause of the offset between the two decay curves observed. These discrepancies outlined are further motivation that this methodolgy alone is not

sufficient, and that Methodology 1 is more suited for removing the pressure drop resulting from adsorption on the surfaces of the dead volume. The majority of the pressure drop from gas expansion is accounted for, but it is not sufficent to yield meaningful upstream pressure decay curves for the purpose of membrane characterization.

### 5.1.2 Zero correction – Methodology 2

The second methodology for correcting the pressure decay curve utilizes the fact that initially the membrane acts as a semi-infinite solid, and the pressure decay curve should initially be a linear function of the square root of time, with an intercept equal to zero as described by Eq. (17). The measured pressure decay can be plotted against the square root of time, and a linear regression can be performed on the initial linear section of the plot, from which the y-intercept can be calculated. Knowing the y-intercept should be zero, any deviation from this value was assumed to be the result of physical phenomena other than gas permeating through the membrane, such as gas expanding into the dead volume and non-instantaneous pressure equilibration within the working volume. The difference between this y-intercept and 0 is the value by which the measured pressure decay curve needs to be shifted along the y-axis to recover the adjusted pressure decay curve.

The same pressure decay curves (already corrected using methodology 1) shown in Figure 16 were plotted in the $\sqrt{t}$ domain and a linear regression was performed for $4 \leq \sqrt{t} \leq 6.5$ and extrapolated the y-axis as shown in Figure 17.

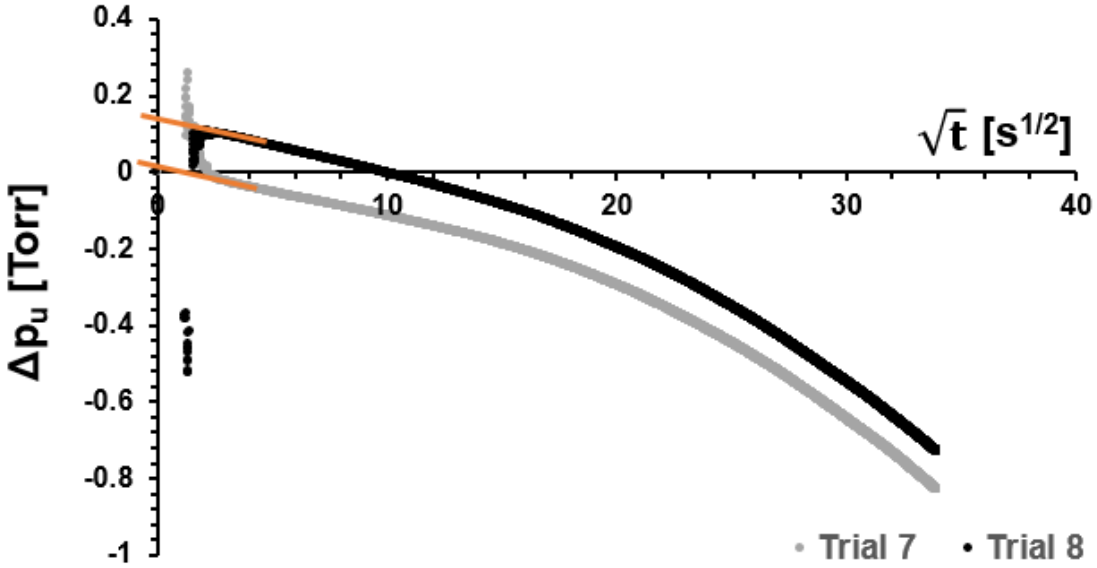


*Figure 17 - Pressure decay curve adjusted using Methodology 1 versus the square root of time for two PPO membrane characterization trials using nitrogen at 1798 Torr and 303 K.*

Subtracting the respective y-intercepts found through the linear regression depicted in Figure 17 from the pressure decay curves already corrected using Methodology 1 represented by Figure 16 yields Figure 18.

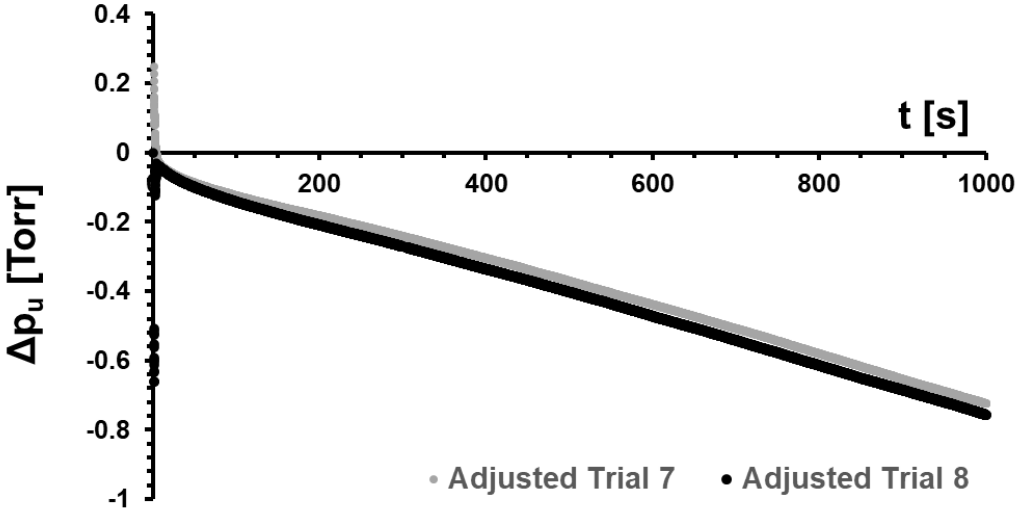


*Figure 18 - Pressure decay curves for nitrogen at 1798 Torr and 303 K permeating through a PPO membrane adjusted using both Methodologies 1 and 2.*

## 5.2 Upstream time lag determination

The upstream time lag was determined using the moving window analysis described in Chapter 3, using the pressure decay curves generated using Eq. (31) and adjusted using either zero correction Methodologies 1 and 2, or just Methodology 2.

## 5.3 Results

A single PPO membrane sample was characterized using upstream pressure decay with multiple feed gases and pressures. Multiple independent trials were performed for each gas and pressure resulting in the experimental matrix outlined in Table 10.

*Table 10 - Upstream pressure decay experimental matrix.*

| Trial | Gas | Pressure [Torr] | Temperature [K] |
|---|---|---|---|
| **1** | Nitrogen | 200.12 | 303.15 |
| **2** | Nitrogen | 199.97 | 303.15 |
| **3** | Nitrogen | 199.94 | 303.15 |
| **4** | Oxygen | 1798.15 | 303.15 |
| **5** | Oxygen | 1797.93 | 303.15 |
| **6** | Oxygen | 1797.8 | 303.15 |
| **7** | Nitrogen | 1798.14 | 303.15 |
| **8** | Nitrogen | 1797.94 | 303.15 |

### 5.3.1 Results using zero correction Methodologies 1 and 2

Using zero correction Methodologies 1 and 2 the pressure decay curves measured from the PPO membrane characterizations trials outlined in Table 10 were corrected and a moving window analysis was used to generate Figure 19, Figure 22, and Figure 23 for trials 1-3, 4-6, and 7-8 respectively.

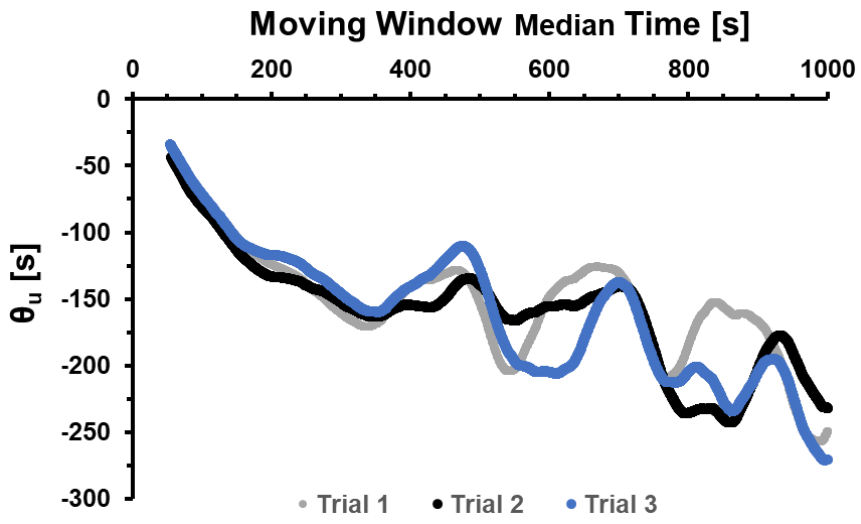


*Figure 19 - Instantaneous time-lag curves characterizing a PPO membrane using nitrogen feed at 194 Torr and 303 K.*

Figure 19 shows that the upstream time lag for all three trials exhibited a similar trend over the course of the time lag experiment. The upstream time lag tends to be more negative (increase in magnitude) as the experiment progresses. This increase in magnitude of $\theta_u$ is what is expected as the feed pressure, and consequently the flux across the membrane decreases resulting in the $dp/dt$ to decrease in magnitude as the experiment progresses. This results in the extrapolated time lag value to continuously becoming more negative. Conversely, using the downstream time-lag method the decrease in slope of the pressure rise curve causes the magnitude of $\theta_d$ to decrease over the course of the trial. This results in the downstream time lag experiencing a plateau, as seen in Figure 9, whereas no such plateau is achieved with upstream time lag method using the window moving analysis. Periodic oscillations are observed in the plot of $\theta_u$ vs $t$. The oscillations observed result from the periodic oscillations in $dp_u/dt$, referring to Eq. (18) the value of $dp_u/dt$ is the sum of three terms, $dn/dt$, $dV/dt$, and $dT/dt$. These oscillations in the quasi-steady state decay curve can be observed in Figure 21.

As mentioned prior the time derivative of temperature within the upstream receiver is significant as it is directly proportional to the pressure within the upstream working volume. As the time lag is calculated by extrapolating a linear regression of the pressure decay curve to the x-axis small changes in the slope result in larger errors as the distance of the extrapolation increases. Due to the continuous decrease in $\theta_u$ and periodic oscillations observed there is no definitive time

to conclude time lag value from using the window moving analysis. Figure 20 shows the conventional methodology of using a straight edge to determine $\theta_u$ from the pressure decay curve after correcting it with Methodologies 1 and 2. Using the straight edge the value of $\theta_u$ was determined to be approximately -140 s, for the same trial $\theta_d$ was determined using the moving window method was 100 s.

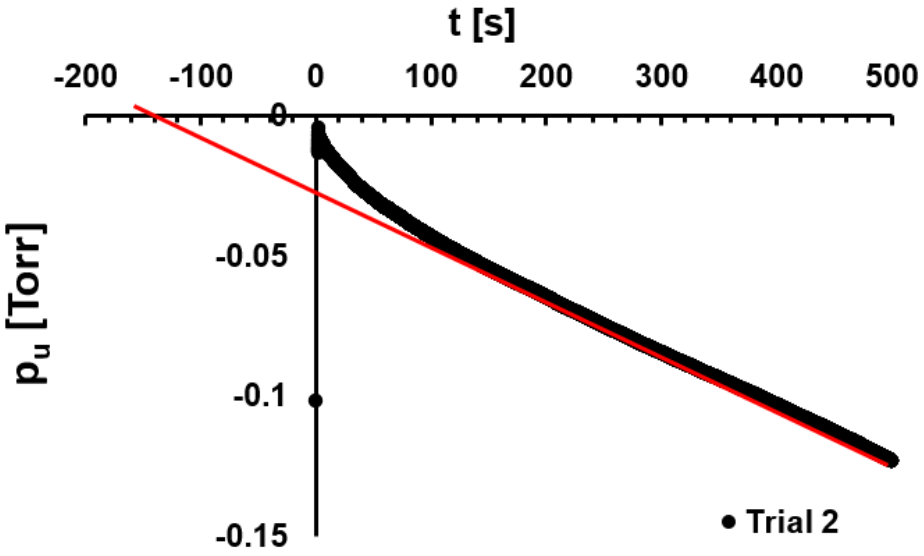


*Figure 20 - Upstream pressure decay - trial 2, nitrogen feed at 194 Torr and 303 K.*

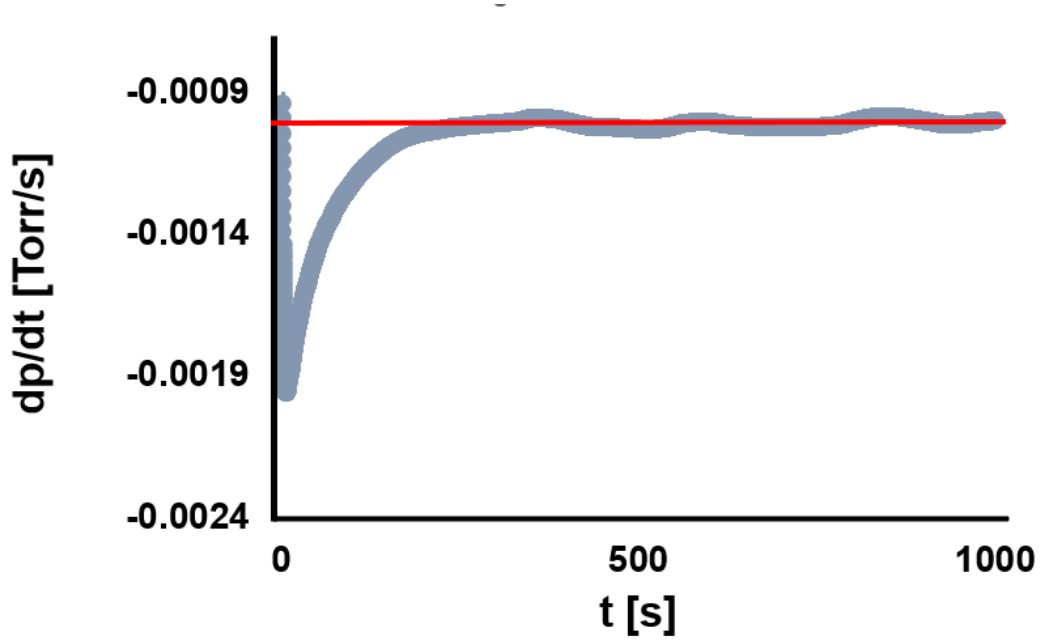


*Figure 21 - Fluctuations in the quasi-steady state slope of the decay curve observed during trial 7, raw data was adjusted using zero-correction Methodology 2 only.*

The next series of window moving analyses was performed on the data collected for trials 4-6 for oxygen permeating through PPO at a feed pressure of 1798 Torr and 303 K illustrated by Figure 22.

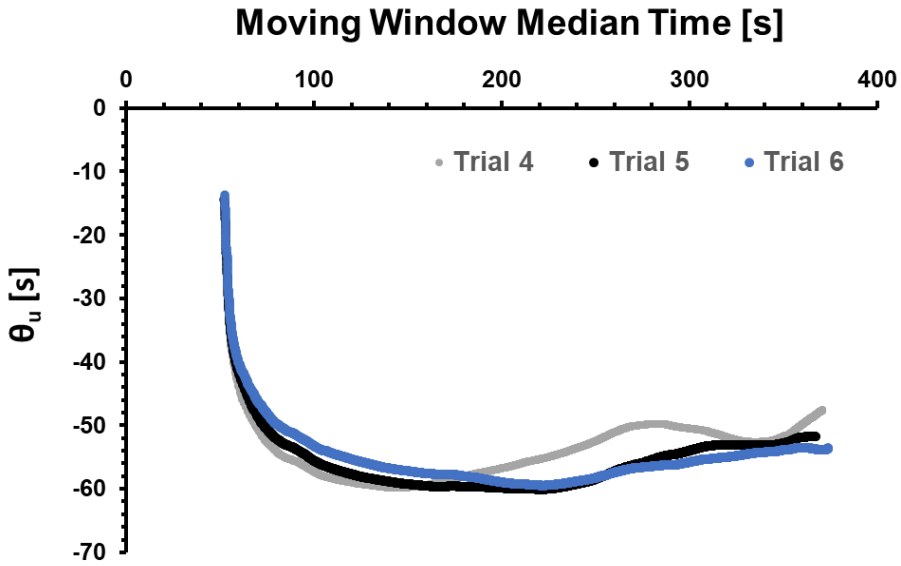


*Figure 22 - Instantaneous time-lag curves characterizing a PPO membrane using oxygen feed at 1798 Torr and 303 K generated by correcting the decay curve using the zero-correction Methodology 1 and 2.*

The instantaneous upstream time lag for trials conducted utilizing oxygen as the feed gas exhibited less noise and a clearer conclusion could be drawn from this set of data in contrast to the data for nitrogen at 200 Torr. Since time lag of oxygen is less than that of nitrogen quasi-steady state behavior is achieved earlier in time, and thus the extrapolations made to the x-axis result in less variability in the observed time lag. Additionally, as the rate of pressure decay is greater for oxygen than in nitrogen, changes in pressure resulting from the time derivative of temperature have a lesser impact on the observed time lag as its quantitatively a smaller fraction of the total time derivative of pressure observed in the working volume. Towards the end of the trial an anomalous upward deviation starts to emerge which is better illustrated by the next trials 7 and 8 depicted in Figure 23.

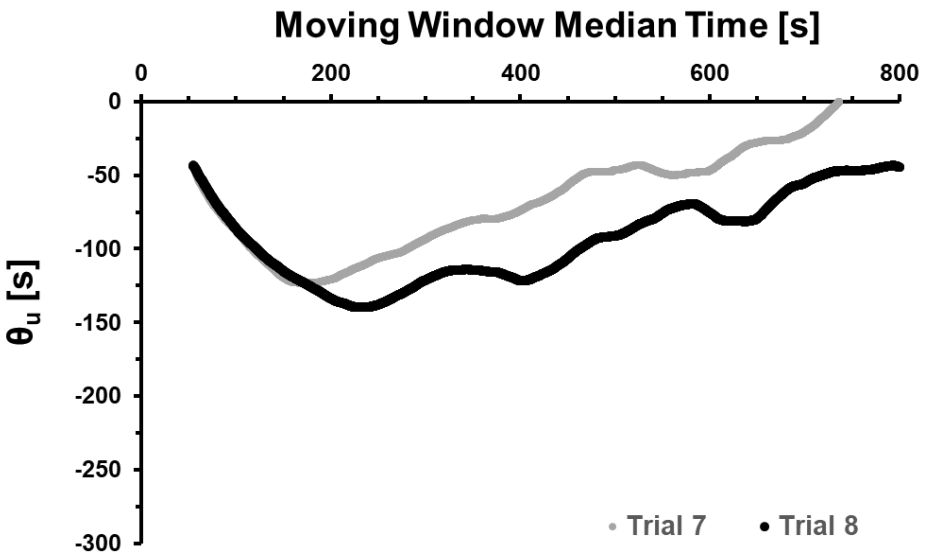


*Figure 23 - Instantaneous time-lag curves characterizing a PPO membrane using a pure nitrogen feed at 1798 Torr and 303 K generated by correcting the decay curve using the zero-correction Methodology 1 and 2.*

The results observed for trials 7 and 8 conducted using nitrogen gas at a feed pressure of 1798 Torr and 303 K and corrected for using Methodologies 1 and 2 for correcting the zero, seen in Figure 23, are anomalous. The instantaneous time lag tends to increase over time, opposite of what is expected, and seen previously in Figure 19. As both independent trials 7 and 8 experienced this atypical behavior it was first hypothesized that this is a result of performing zero correction Methodology 1 and not the result of physical phenomena. Further investigation reveals that when the raw data is only adjusted using zero-correction Methodology 2, that only leverages the linear intercept determined through fitting Eq. (17) to the pressure decay curve as depicted in Figure 17, that this trend of increasing upstream time lag is not observed, as seen in Figure 26. This leads to the conclusion that what caused the upward deviation of the time lag was not recorded during the membrane characterization trial and was a result of applying zero-correction Methodology 1.

### 5.3.2 Results using zero-correction Methodology 2

Using only zero-correction Methodology 2 the pressure decay curves measured from the PPO membrane characterizations tests outlined in Table 10 were corrected and a moving window analysis was used to generate Figure 24, Figure 25, and Figure 26 for trials 1-3, 4-6, and 7-8

respectively.

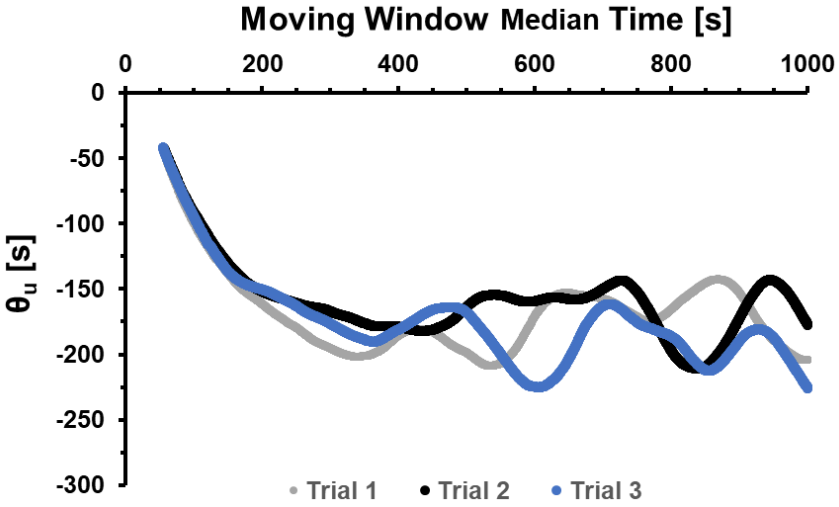


*Figure 24 - Instantaneous upstream time-lag curves characterizing a PPO membrane using a nitrogen feed at 194 Torr and 303 K generated by correcting the decay curve using the zero-correction Methodology 2 exclusively.*

Like Figure 19, Figure 24 exhibits periodic oscillations in the upstream time lag value resulting from the time derivative of temperature causing a cyclical rise and fall in the slope of the decay curve and the resulting extrapolation error.

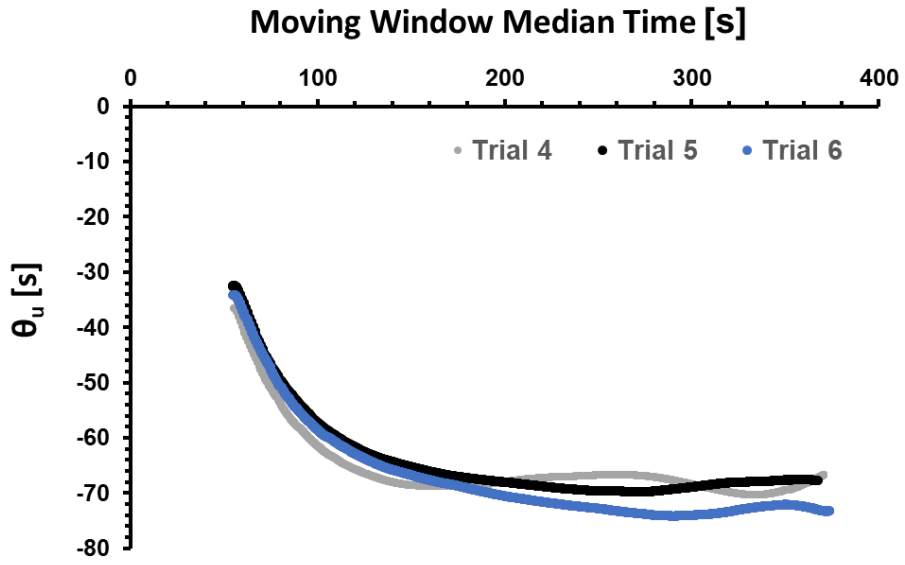


*Figure 25 - Instantaneous upstream time-lag curves characterizing a PPO membrane using an oxygen feed at 1798 Torr and 303 K generated by correcting the decay curve using the zero-correction Methodology 2 exclusively.*

Similarly, to the plot generated previously for $\theta_u$ vs $t$ for trials 4-6 that was corrected using both Methodologies 1 and 2, the plot corrected using only the Methodology 2 also exhibited less variability in the time lag due to the shorter run duration and increased rate of pressure decay. Contrasting Figure 25 with Figure 22, originating from the same raw data but differing in correction methodologies, the anomalous upward deviation is not observed at the end of the trial. The upward deviation observed prior must originate from the data collected during the calibration run and not something observed during the membrane characterization trial.

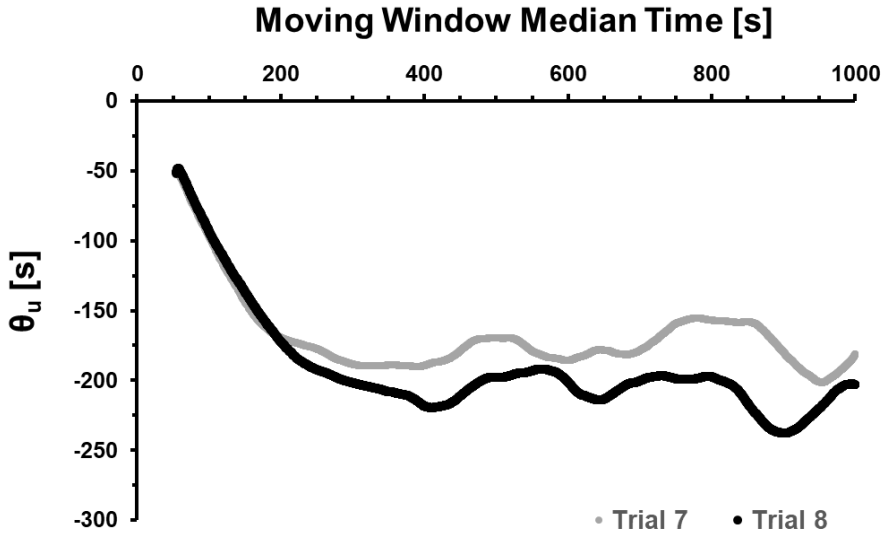


*Figure 26 - Instantaneous time-lag curves characterizing a PPO membrane using a nitrogen feed at 1798 Torr and 303 K generated by correcting the decay curve using the zero-correction Methodology 2 exclusively.*

### 5.4 Discussion

A summary of the upstream time lag and permeability coefficients determined using the window method analysis for trials 1-8 are presented along-side the values determined downstream of the membrane for the same trials. It should be noted that in each row the values measured using the upstream and downstream time lag methods was observed simultaneously and correspond to a single experiment. Values of $\theta_u$, and $P_u$ reported were not selectively chosen from the figures reported in this chapter to achieve values in agreeance with the anticipated results. Instead, the median time was selected by visual inspection of $\theta_d$ vs $t$ and inferring at what time the plateau in $\theta_d$ occurred, as previously illustrated by Figure 9. The values of $\theta_u$, and $P_u$ were then reported at the same median time as was selected during the downstream analysis. The upstream and

downstream values reported were determined using linear regression, with a time interval of 100 s with the median time of 500 s, 150 s, and 400 s for trials 1-3, 4-6, and 7-8 respectively.

Table 11 shows a summary of time lags and permeabilities for data collected and corrected using zero-correction Methodology 1and 2 whereas Table 12 shows the data corrected using Methodology 2 exclusively.

*Table 11 - Permeabilities and time lags determined using downstream pressure rise, and upstream pressure decay with data corrected using zero-correction Methodologies 1 and 2.*

| Trial | $P_u$ [Barrer] | $P_d$ [Barrer] | $P_u/P_d$ | $\theta_u$ [s] | $\theta_d$ [s] | $\theta_u/\theta_d$ |
|---|---|---|---|---|---|---|
| **1** | 3.72 | 3.15 | 1.18 | -201.80 | 102.96 | -1.96 |
| **2** | 4.41 | 3.32 | 1.33 | -166.03 | 100.07 | -1.66 |
| **3** | 4.15 | 3.38 | 1.23 | -197.00 | 96.82 | -2.03 |
| **4** | 8.39 | 13.84 | 0.61 | -56.73 | 33.89 | -1.67 |
| **5** | 8.33 | 13.73 | 0.61 | -59.82 | 33.78 | -1.77 |
| **6** | 8.37 | 13.88 | 0.60 | -58.93 | 33.92 | -1.74 |
| **7** | 1.74 | 2.86 | 0.61 | -178.00 | 115.57 | -1.54 |
| **8** | 1.69 | 2.86 | 0.59 | -218.76 | 115.78 | -1.89 |

*Table 12 - Permeabilities and time lags determined using downstream pressure rise, and upstream pressure decay with data corrected using zero-correction Methodology 2 only.*

| Trial | $P_u$ [Barrer] | $P_d$ [Barrer] | $P_u/P_d$ | $\theta_u$ [s] | $\theta_d$ [s] | $\theta_u/\theta_d$ |
|---|---|---|---|---|---|---|
| **1** | 3.89 | 3.15 | 1.23 | -206.03 | 102.96 | -2.00 |
| **2** | 4.58 | 3.32 | 1.38 | -154.74 | 100.07 | -1.55 |
| **3** | 4.32 | 3.38 | 1.28 | -200.43 | 96.82 | -2.07 |
| **4** | 9.44 | 13.84 | 0.68 | -67.94 | 33.89 | -2.00 |
| **5** | 9.38 | 13.73 | 0.68 | -67.88 | 33.78 | -2.01 |
| **6** | 9.42 | 13.88 | 0.68 | -70.51 | 33.92 | -2.08 |
| **7** | 2.62 | 2.86 | 0.92 | -178.00 | 115.57 | -1.54 |
| **8** | 2.58 | 2.86 | 0.90 | -218.76 | 115.78 | -1.89 |

Inspection of Table 1 shows that the upstream time lags calculated for the trials where nitrogen was used (trials 1-3 and 7-8) experience much greater variability than those trials

conducted for oxygen. The magnitude of $\theta_u/\theta_d$ was less than 2 for the analysis performed on data corrected using both zero-correction Methodologies, whereas the ratios calculated using Methodology 2 yielded values greater than 2. This is because decreasing the rate of adsorption decreases the magnitude of *dp/dt* and thus a more negative time lag is extrapolated from the decay curve. The expected magnitude of the ratio of $\theta_u/\theta_d$ being equal to 2 represents the limiting case where Henry's law is applicable, however since PPO is a glassy polymer it exhibits non-linear sorption isotherms [30], which has the effect of decreasing the magnitude of $\theta_u/\theta_d$ below 2 at none zero pressures [31]. It should be reiterated that these values of $\theta_u$ are highly variable due to the *dT/dt* contribution, and no claim is being made that this is a true measure of the value of $\theta_u$.

The ratio of upstream and downstream permeability should be equal to 1 [17] but trials conducted at higher pressures yielded a value significantly less than 1. This error is not a consequence of a leak in the system, as above atmospheric pressures a leak would cause an increased value of $P_u$ as *dp/dT* would be increased. Additionally, the system was repeatedly leak tested and it was determined that negligible leaks existed, as discussed in Chapter 2. This was investigated when trouble-shooting the system initially after construction, and always observed during every upstream pressure decay test conducted. It should be noted that the two upstream volumes are isolated with the valve FCV-1 as shown in Figure 2. It was verified experimentally that the correlation of the pressure within the working ($V_w$) and reference volumes ($V_r$) could only be attributed to the DPT. When the DPT was removed, and the connections were capped in its place, the correlation between the pressures within $V_w$ and $V_r$ could no longer be reproduced. The differential pressure transducer operates by measuring the change in capacitance resulting from the deflection of a metal diaphragm which compares pressures within the $V_w$ and $V_r$. Due to the large diameter of this diaphragm a small displacement causes a significant change in volume within both $V_w$ and $V_r$. As the pressure within the $V_W$ decreases due to gas permeation, less force is applied on the diaphragm and it shifts towards $V_w$ causing a reduction in its volume, thereby increasing $V_r$. This was independently verified by CCR Process Products in Kanata Ontario, who supplied the DPT. In an email correspondence, see Appendix A, it was verified by another lab that the displacement of this diaphragm can result in a volume change equal to about 0.5 $cm^3$. Although 0.5 $cm^3$ may seem insignificant, $V_w$, which includes the dead volume in the membrane cell, is only 96.55 $cm^3$ thus 0.5 $cm^3$ is a non-negligible change. The change in volume within both upstream volumes has a dual effect of decreasing the measured pressure decay by the DPT. Firstly, an

increase in volume within $V_r$ causes a decrease in pressure within $V_r$, thus when the pressure differential is taken between the $V_w$ and $V_r$ value is less by the amount of pressure drop experienced within $V_r$. Secondly, the decrease in $V_w$ over time results in a positive contribution to *dp/dt* within the working volume (Eq. (18)), decreasing the perceived permeability as the two are directly proportional.

The pressure drop within $V_w$ and $V_w$ over the course of a typical time lag experiment can be seen in Figure 27, Figure 28 and Figure 29 which corresponds to trials 3, 4, and 7 respectively.

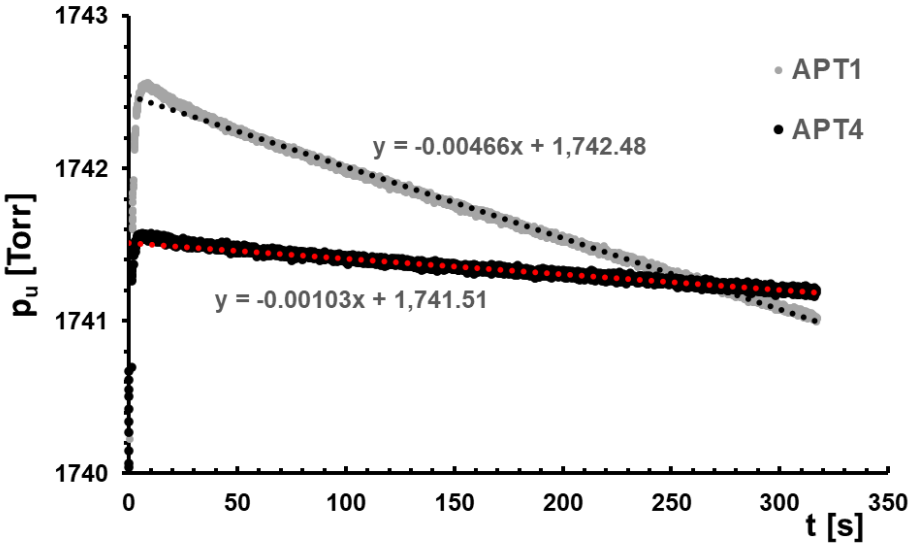


*Figure 27 - Pressure measured by $APT_1$ and $APT_4$ in the working and reference volumes respectively over the course of a PPO membrane characterization trial conducted with oxygen gas at 1798 Torr and 303 K.*

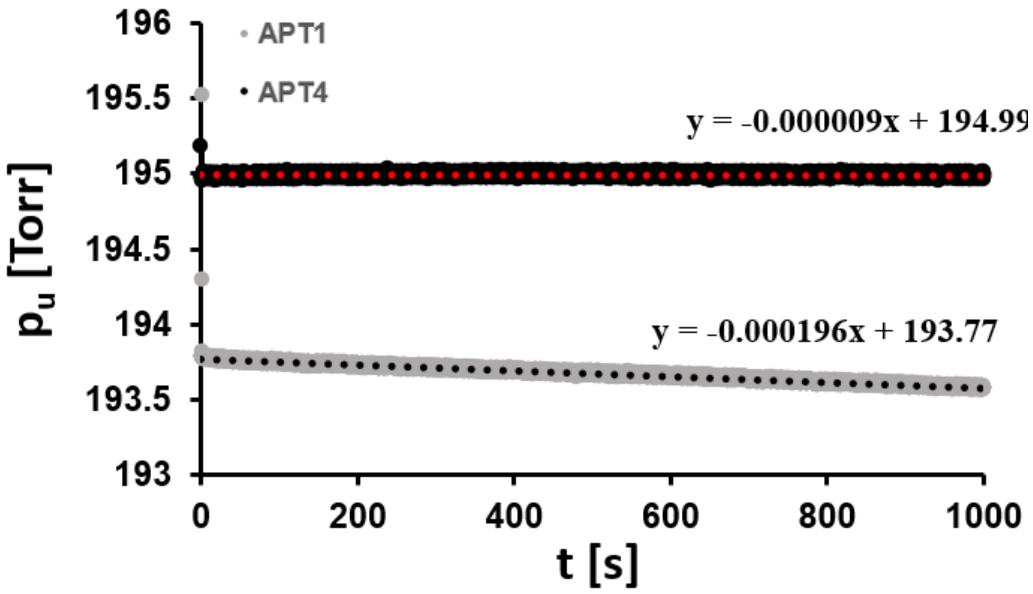


*Figure 28 - Pressure measured by $APT_1$ and $APT_4$ in the working and reference volumes respectively over the course of a PPO membrane characterization trial conducted with nitrogen gas at 194 Torr and 303 K.*

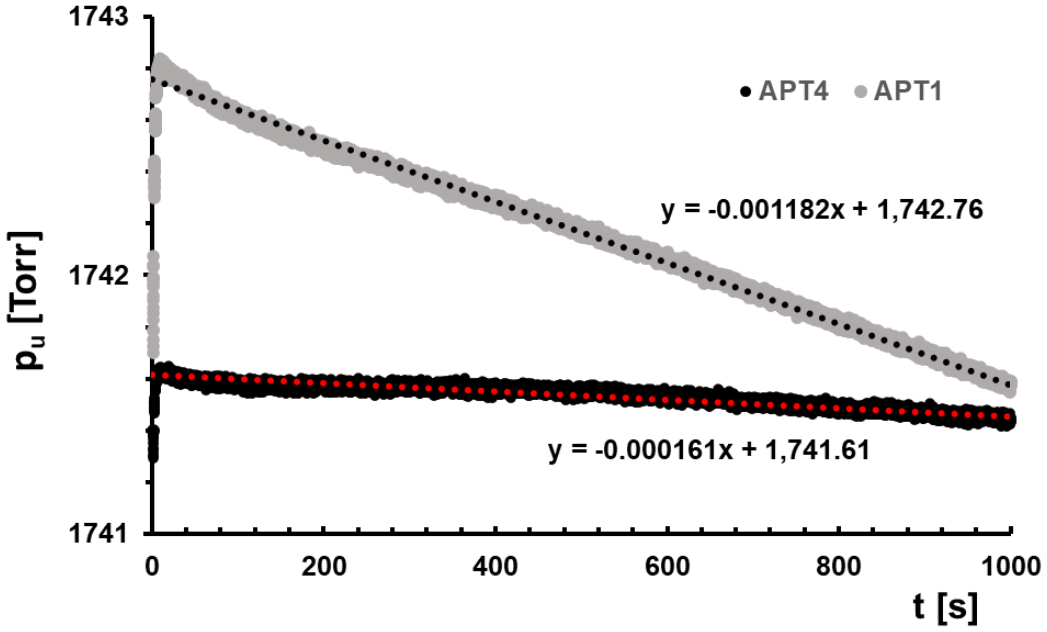


*Figure 29 - Pressure measured by $APT_1$ and $APT_4$ in the working and reference volumes respectively over the course of a PPO membrane characterization trial conducted with nitrogen gas at 1798 Torr and 303 K.*

It was found that the ratio between $dp/dt$ in $V_w$ and $V_r$ is not a fixed ratio but is always observed. For the case of nitrogen gas at 200 Torr, the pressure decay within the reference volume was only $9\times10^{-6}$ Torr/s, which is relatively small the rate of pressure decay within the working volume that was $1.6\times10^{-4}$ compared to the trials conducted at 1798 Torr. Recalling Table 11 and Table 12 the trials conducted at 200 Torr exhibited a $P_u/P_d$ ratio greater than 1, unlike trials at 1798 Torr that experience a greater relative reduction in pressure within the reference volume. $P_u/P_d$ being greater than 1 could be a result of error in measuring the volumes of the receiver. If observed value of $dp/dt$ was not decreased due to the DPT it would result in a steeper decay curve, and the observed upstream time lag values would decrease in magnitude. This would bring the magnitude of $\theta_u/\theta_d$ observed below 2, which is the limiting ideal case for polymers exhibiting linear sorption isotherms.

## 6.0 Overall Conclusions and Recommendations

The time lag contribution of the downstream receiver was quantified and deemed to be non-negligible for any configuration other than those consisting of a single large diameter 12.7 mm (1/2”) OD tube. It is suggested that all membranes characterized with this CV system, and CV systems in general, is done without the use of accumulation tanks, as those amplifying the resistances experienced within the tubing connecting the membrane cell and accumulation tanks. Utilizing a system with a large time lag contribution would result in the transport properties determined for the material to be incorrect. Diffusivity and solubility coefficients were found to be more susceptible to error resulting from the time lag contribution of the receiver. Measures of permeability were found to be less affected by the resistance to gas accumulation. The time lag contributions of the receiver measured agreed qualitatively with the model developed by S. Lashkari but were measured to be greater than predicted. Adding volumes to the receiver results in large negative time lag contributions which result in overestimations of diffusivity and underestimations on the solubility of a gas within a membrane sample. These observations were determined to be statistically significant. It is hypothesized that the observed resistance being greater than that predicted is a result of additional resistances imposed upon the receiver from tee connections and bends within the tubing. To test this hypothesis, it is suggested that a downstream receiver be constructed from a singular tube that is purposely tortuous and compare it against a receiver with the same length of tubing but with no tees or bends.

The current iteration of the constant volume system can precisely determine the three transport coefficients, $P$, $D$ and $S$ using a single dynamic gas permeation experiment by monitoring the downstream pressure response. Additionally, the temperature at which the experiment is performed can now be varied, which allows for the determination of the activation energy of permeation, diffusion, and the enthalpy of solution. PPO was characterized using both oxygen and nitrogen gas at various temperatures and it was determined that the perspectivity of oxygen over nitrogen is negatively correlated to the temperature of the gas. The current CV system is capable of characterizing membranes at pressures up to 2000 Torr and between 273-313 K. The pressure range at which experiments can be performed can easily be expanded by switching the absolute pressure transducers in the upstream sections. A current limitation of the system is the lack of inline temperature measurements. Temperatures were estimated as the average value of minimum and maximum air temperatures measured within the enclosure housing the CV system. The

temperature variations within the system are likely to be less, as currently the system is insulated with ½" closed cell polyethylene pipe insulation. It is recommended to instal thermocouples within the working and reference volumes, so that they can independently be monitored. Temperature measurements within the downstream are not deemed necessary due to the low pressures within this section of the CV system.

Time lag experiments leveraging upstream pressure decay were performed and time lag, and permeability can be measured after correcting the origin of the pressure decay response. The time lags and permeabilities measured using upstream pressure decay tests revealed inadequacy in the performance of the system. The magnitude of the ratio of upstream to downstream time lag was observed to be greater than 2, which is not possible for a polymer governed by the solution diffusion theory, even in the most ideal case where the polymer/gas system exhibit a linear sorption isotherm. Additionally, the ratio of measured upstream and downstream permeability was not equal to 1. This was determined the be a result of the mechanism by which a differential pressure transducer measures the pressure differential between the working and reference volumes. A decrease in the pressure within the working volumes causes a decrease in pressure within the reference volume, as the diaphragm within the DPT shifts. This has the effect of reducing the pressure differential measured, as the pressures reduce in tandem in both volumes, which is detracting from the pressure decay and is measured as a lower permeability. Additionally, the shifting diaphragm represents a negative time derivative of volume, which too results in decreased perceived permeability. To partially rectify the first half of this problem, the variable reference pressure, it is suggested to install and excessively large reference volume in comparison to the working volume. Currently the working and reference volumes are similar, it is proposed that the reference volume be increased by two orders of magnitude, to approximately 10 L. This modification to the system would help keep the reference pressure more stable, as proportionally a change in volume of 0.005 L would be a significantly less than it currently is. The decrease in volume within the working volume is unavoidable, as using a large volume decreases the sensitivity of the CV system. It is proposed that a model be developed using empirical data to correct for this change in volume post hoc.

Currently temperature variation within the CV system results in a large degree of variability of the measured upstream time lag value when time lags exceed 60 s. It is recommended that the R factor of the insulation be increased by an order of magnitude to further minimize the

temperature variation. This could be achieved by mounting the CV system on an elevated platform which is well insulated underneath, and by blanketing the entirety of the CV system with 10” or more of semi ridged mineral wool batt insulation. Additionally, if inline thermocouples are installed as previously recommended the temperature variation could be accounted for post hoc.

The final recommendation in relation to performing upstream pressure decay tests is to utilize a rubbery polymer sample when calibrating the system. This would provide the advantage that a linear sorption isotherm would govern the solution of gas within the membrane, and the ratio of upstream to downstream time lags would be known to be 2. The ratio of time lags, and ratio of permeabilities will offer the tools to ensure the system is well calibrated and that upstream time lag experiments are providing accurate results.

## 7.0 References


[1] L.M. Robeson, Z.P. Smith, B.D. Freeman, D.R. Paul, Contributions of diffusion and solubility selectivity to the upper bound analysis for glassy gas separation membranes, J Memb Sci. 453 (2014) 71–83. https://doi.org/10.1016/j.memsci.2013.10.066.

[2] R.W. Baker, Future directions of membrane gas separation technology, Ind Eng Chem Res. 41 (2002) 1393–1411. https://doi.org/10.1021/ie0108088.

[3] R.W. Baker, K. Lokhandwala, Natural gas processing with membranes: An overview, Ind Eng Chem Res. 47 (2008) 2109–2121. https://doi.org/10.1021/ie071083w.

[4] R. Prasad, F. Notaro, D.R. Thompson, Evolution of membranes in commercial air separation, J Memb Sci. 94 (1994) 225–248. https://doi.org/10.1016/0376-7388(93)E0193-N.

[5] D.F. Sanders, Z.P. Smith, R. Guo, L.M. Robeson, J.E. McGrath, D.R. Paul, B.D. Freeman, Energy-efficient polymeric gas separation membranes for a sustainable future: A review, Polymer (Guildf). 54 (2013) 4729–4761. https://doi.org/10.1016/j.polymer.2013.05.075.

[6] Q. Wang, R. Zhou, T. Tsuru, Recent Progress in Silicon Carbide-Based Membranes for Gas Separation, Membranes (Basel). 12 (2022). https://doi.org/10.3390/membranes12121255.

[7] A.R. Kamble, C.M. Patel, Z.V.P. Murthy, A review on the recent advances in mixed matrix membranes for gas separation processes, Renewable and Sustainable Energy Reviews. 145 (2021) 111062. https://doi.org/10.1016/j.rser.2021.111062.

[8] L.M. Robeson, The upper bound revisited, J Memb Sci. 320 (2008) 390–400. https://doi.org/10.1016/j.memsci.2008.04.030.

[9] H.A. Daynes, The process of diffusion through a rubber membrane, Proceedings of the Royal Society of London. Series A, Containing Papers of a Mathematical and Physical Character. 97 (1920) 286–307. https://doi.org/10.1098/rspa.1920.0034.

[11] A.T.D. D.R. Paul, Diffusion in amorphous polymers, J. Polym. Sci. Part C. 10 (1965) 17–44.

[12] S.W. Rutherford, D.D. Do, Review of time lag permeation technique as a method for characterisation of porous media and membranes, Adsorption. 3 (1997) 283–312. https://doi.org/10.1007/BF01653631.

[13] J.A. Barrie, H.G. Spencer, A. Quig, Transient diffusion through a membrane separating finite and semi-infinite volumes, Journal of the Chemical Society, Faraday Transactions 1: Physical Chemistry in Condensed Phases. 71 (1975) 2459–2467.

https://doi.org/10.1039/F19757102459.

[14] L.S. R. C. LL. Jenkins P. M. Nelson, Calculation of the Transient Diffusion of a Gas through a Solid Membrane into a Finite Outflow Volume, Transactions of the Faraday Society. 66 (1970) 1391–1401.

[15] H. Wu, B. Kruczek, J. Thibault, Impact of measuring devices and data analysis on the determination of gas membrane properties, Journal of Membrane Science and Research. 4 (2018). https://doi.org/10.22079/jmsr.2017.63433.1136.

[16] N. Al-Qasas, J. Thibault, B. Kruczek, The effect of the downstream pressure accumulation on the time-lag accuracy for membranes with non-linear isotherms, J Memb Sci. 511 (2016). https://doi.org/10.1016/j.memsci.2016.03.047.

[17] H. Wu, Gas membrane characterization via the time-lag method for neat and mixed-matrix membranes, Doctoral dissertation, University of Ottawa, 2020.

[18] B. Kruczek, H.L. Frisch, R. Chapanian, Analytical solution for the effective time lag of a membrane in a permeate tube collector in which Knudsen flow regime exists, J Memb Sci. 256 (2005). https://doi.org/10.1016/j.memsci.2005.02.006.

[19] S. Lashkari, B. Kruczek, H.L. Frisch, General solution for the time lag of a single-tank receiver in the Knudsen flow regime and its implications for the receiver's configuration, J Memb Sci. 283 (2006). https://doi.org/10.1016/j.memsci.2006.06.015.

[20] S. Lashkari, B. Kruczek, Effect of resistance to gas accumulation in multi-tank receivers on membrane characterization by the time lag method. Analytical approach for optimization of the receiver, J Memb Sci. 360 (2010). https://doi.org/10.1016/j.memsci.2010.05.043.

[21] K. Mizrahi Rodriguez, W.N. Wu, T. Alebrahim, Y. Cao, B.D. Freeman, D. Harrigan, M. Jhalaria, A. Kratochvil, S. Kumar, W.H. Lee, Y.M. Lee, H. Lin, J.M. Richardson, Q. Song, B. Sundell, R. Thür, I. Vankelecom, A. Wang, L. Wang, C. Wiscount, Z.P. Smith, Multi-lab study on the pure-gas permeation of commercial polysulfone (PSf) membranes: Measurement standards and best practices, J Memb Sci. 659 (2022) 120746. https://doi.org/10.1016/j.memsci.2022.120746.

[22] X.Q. Nguyen, Z. Brož, F. Vašák, Q.T. Nguyen, Manometric techniques for determination of gas transport parameters in membranes. Application to the study of dense and asymmetric poly(vinyltrimethylsilane) membranes, J Memb Sci. 91 (1994) 65–76. https://doi.org/10.1016/0376-7388(94)00019-0.

[23] M. Al-Ismaily, J.G. Wijmans, B. Kruczek, A shortcut method for faster determination of permeability coefficient from time lag experiments, J Memb Sci. 423–424 (2012). https://doi.org/10.1016/j.memsci.2012.08.009.

[24] N. Al-Qasas, J. Thibault, B. Kruczek, Analysis of gas transport in laminated semi-infinite solid: Novel method for complete membrane characterization during highly transient state, J Memb Sci. 460 (2014). https://doi.org/10.1016/j.memsci.2014.02.024.

[25] N. Al-Qasas, J. Thibault, B. Kruczek, Membrane Characterization Based on the Upstream Pressure Decay in a Dynamic Gas Permeation Test, J Fluid Flow Heat Mass Transf. 1 (2014) 57–64. https://doi.org/10.11159/jffhmt.2014.009.

[26] M. Sadrzadeh, M. Rezakazemi, T. Mohammadi, Fundamentals and Measurement Techniques for Gas Transport in Polymers, Elsevier Inc., 2017. https://doi.org/10.1016/B978-0-12-809884-4.00019-7.

[27] E.B. Arkilic, M.A. Schmidt, K.S. Breuer, Gaseous slip flow in long microchannels, Journal of Microelectromechanical Systems. 6 (1997) 167–178. https://doi.org/10.1109/84.585795.

[28] H. J. Seltman, Experimental Design and Analysis, Carnegie Mellon University, 2018.

[29] K. Haraya, S.T Hwang, Permeation of oxygen, argon and nitrogen through polymer membranes, J. Memb. Sci. 71 (1992) 13-27. https://doi.org/10.1016/0376-7388(92)85002-Z.

[30] Y. Huang, H. Cai, T. Yu, X. Sun, B. Tu, and D. Zhao, Highly Ordered Mesoporous Carbonaceous Frameworks from a Template of a Mixed Amphiphilic Triblock-Copolymer System of PEO–PPO–PEO and Reverse PPO–PEO–PPO. Chemistry – An Asian Journal, 2(2007): 1282-1289. https://doi.org/10.1002/asia.200700173.

[31] N. Al-Qasas, J. Thibault, B. Kruczek, A new characterization method of membranes with nonlinear sorption isotherm systems based on continuous upstream and downstream time-lag measurements, J Memb Sci. 542 (2017). https://doi.org/10.1016/j.memsci.2017.07.039.

## Appendix A – Email Correspondence

**From:** Claude Martel
**Sent:** July 9, 2019 8:35 AM
**To:** Boguslaw Kruczek Haoyu Wu
**Cc:** Peter Leszczynski Steve Wright
**Subject:** RE: MKS 698A inquiries

Attention : courriel externe | external email
Hello Bogdan,

Looks like this is the way the instrument works. We checked another Baratron here and it gives about a 0.5 cc change in volume. Since the diaphragm is fairly large in area, even a very small change in distance still represents a measurable volume. Unusual application, but you'll have to try to take this into consideration in your measurements. MKS won't give me the exact measurements as they consider that proprietary, but it's fairly easy to measure anyway.

Please advise. Thanks.
Claude